Ore Geology Reviews 153 (2023) 105272

Contents lists available at ScienceDirect

Ore Geology Reviews

journal homepage: www.elsevier.com/locate/oregeorev

U-Pb detrital zircon ages and Hf isotope from Sardinia and Adria Cretaceous bauxite (Italy): Constraints on the Alpine Tethys paleogeography and tectonic evolution

Wenchao Yu [a,b,*], Giacomo Oggiano [c], Giovanni Mongelli [d], Jintao Zhou [a,b], Roberto Buccione [d], Lingtong Xu [a,b], Paola Mameli [c], Yuansheng Du [a,b]

[a] State Key Laboratory of Geological Processes and Mineral Resources, School of Earth Sciences, China University of Geosciences-Wuhan, Wuhan 430074, China
[b] Innovation Center of Ore Resources Exploration Technology in the Region of Bedrock, Ministry of Natural Resources of People's Republic of China, Guiyang 550004, China
[c] Dipartimento di Scienze Matematiche, Fisiche e Naturali Università di Sassari, Sassari 07100, Italy
[d] Dipartimento di Scienze, Università della Basilicata, Potenza 85100, Italy

ARTICLE INFO

Keywords:
Geochronology
Parental affinities
Weathering
Neotethys

ABSTRACT

Bauxite deposits in Italy mainly distribute in Sardinia and Adria regions within Cretaceous carbonate sequences. Parental affinity of Italian bauxite deposits has long been a controversial problem. At least four potential sources have been proposed: (1) Cretaceous debris and autochthonous marlstones; (2) alluvial sheets from the weathered Variscan basement; (3) weathering materials from North Africa and (4) Cretaceous bimodal volcanism in the Dinaric and Carpatho-Balkan orogenic belts. In this study, a total of 374 detrital zircon U-Pb ages and 86 Hf isotope values have been acquired from Cretaceous bauxites of Sardinia and Adria regions. Combining with the published geochemical data, provenances of Cretaceous bauxite deposits in Sardinia and Adria regions have been discussed. In bauxite deposits of Sardinia, dominant Early Paleozoic aged zircon grains (main age peaks at 291 – 295 Ma, 454 – 465 Ma, and 582 – 639 Ma) and their various Hf isotope compositions ($\varepsilon Hf(t) = +9.61$ to -5.66) indicate a parental affinity of Variscan metasedimentary basement. As a contrast, bauxite deposits in Adria show abundant Jurassic – Cretaceous (93 – 178 Ma) zircon grains with negative $\varepsilon Hf(t)$ values (-13.75 to −4.61), demonstrating significant supply from coeval volcanic materials. Cretaceous bauxite samples from Sardinia and Adria shed light on paleogeographic restoration and tectonic evolution of Alpine Tethys. Began in Early Cretaceous, Sardinia was affected by uplift due to the subduction between Ligurian oceanic crust and the Iberia plate. The Mesozoic carbonate sequence were eroded and the underlying Variscan basement was exposed in the area from Sardinia to the Massif Meridional, provided weathering materials for bauxitization. Late Cretaceous witnessed the further NNE-trending subduction of the Adria Plate to the West Vardar oceanic plate, where calcalkaline igneous rocks and volcanic ashes from Dinarides supplied windborne weathering materials to carbonate platforms in Adria. Particularly, provenance difference between the bauxite of central-southern Apennine and Sardinian reveals that the hosting carbonate sequence in Apennine was not located on the Sardinia shelf before the Cenozoic tectonism in the south Mediterranean realm. Diversity of provenances in bauxite deposits from Sardinia and Adria may cause differences in geochemical composition and further influence qualities of bauxite ore in two regions.

1. Introduction

Bauxite is a kind of weathering residue in the subaerial environment in tropical and subtropical regions (D'Argenio and Mindszenty, 1995; Price et al., 1997; Yu et al., 2019). It is conventional to divide bauxite deposit into three main types: (1) karst-type, for those overly on the carbonate bedrocks; (2) laterite-type, bauxite deposits cover the aluminosilicate bedrocks; and (3) sedimentary-type, bauxite deposits

* Corresponding author at: State Key Laboratory of Geological Processes and Mineral Resources, School of Earth Sciences, China University of Geosciences-Wuhan, Wuhan 430074, China.
E-mail address: yuwenchaocug@163.com (W. Yu).

https://doi.org/10.1016/j.oregeorev.2022.105272
Received 8 September 2022; Received in revised form 19 November 2022; Accepted 21 December 2022
Available online 23 December 2022

cover the aluminosilicate bedrocks but they went through obvious transport process (Bárdossy, 1982). Besides economic significance of bauxite (the dominant aluminum metal source), this deposit has been treated as a typical tectonic uplift and warm and humid (paleo-)climate indicator (Bárdossy and Combes, 1999). Strong chemical weathering processes during the formation of bauxite lead to the enrichments of Al, Ti, Fe and several trace elements (e.g., Mongelli et al., 2021 and references therein) and leaching of mobile elements (Young and Nesbitt, 1998). These processes cause a long-lasting problem when tracing the source rocks of bauxite deposits, for most provenance information in the bauxite deposits may have been eliminated (Bárdossy, 1982; Yu et al., 2016). To rebuilt the source – sink system for bauxite deposits, several methods have been proposed, the common ones include the element geochemical discrimination method and the heavy mineral tracing method. The former uses weathering-resistant element(s) (e.g., Ti, Zr, Nb, Ta, and REE) within the bauxite deposit and potential source rocks to reconstruct the parental affinity (Abedini et al., 2021; MacLean et al., 1997; Mongelli et al., 2014; Mameli et al., 2020; Weng et al., 2019; Abedini et al., 2022, 2020; Khosravi et al., 2017). The latter compares features of weathering-resisted heavy minerals (e.g., type, assembly, and age) in the bauxite deposit and the potential source rocks, to solve the parent rock(s) problem (Hartman, 1955; Sudom and St. Arnaud, 1971).

Recently, detrital zircon U-Pb aging method has been applied in solving the provenance problems of bauxite deposits in the Chinese Bauxite Province, including the South China Block (Deng et al., 2010; Gu et al., 2013; Hou et al., 2017; Xiong et al., 2021; Yu et al., 2016; Zhou et al., 2022) and the North China Block (Liu et al., 2014; Wang et al., 2016; Wang et al., 2010b; Yang et al., 2018). These studies reveal the complicated provenance system during the Carboniferous – Permian bauxitization of the bauxite deposits in China, the source rocks can be the adjacent orogeny (Wang et al., 2016; Liu et al., 2022), the underlying aluminosilicate rocks (Gu et al., 2013) and the distant volcanic ash (Yu et al., 2016; Wang et al., 2020). For Italian bauxite deposits, however, previous geochronological studies report limited detrital zircon age data (Boni et al., 2012; Mongelli et al., 2016). Insufficient geochronological data hinder the further study on the source rock, paleogeographic reconstruction and tectonic evolution of this region.

Mediterranean Bauxite Province is one of the well-studied bauxite provinces in the world (Bárdossy, 1982; Bogatyrev and Zhukov, 2009), this bauxite province is closely linked with the tectonic evolution and paleoclimate condition of western Neotethys (Combes et al.1993; Combes and Bárdossy, 1996; Mindszenty et al., 1995). As the important part of the Mediterranean Bauxite Province, Italy contains Cretaceous (autochthonous) and Cenozoic (allochthonous) karst-type bauxite deposits (Mongelli et al., 2015). Multiple layers of bauxite deposits are preserved in the Cretaceous shallow-water carbonate platform sequence in Southern Italy, representing the regional unconformities (Mindszenty et al., 1995). Cenozoic bauxite deposit (Salento-type, a subtype of the karstic bauxite deposit, indicating the erosion and redeposition of pre-existed bauxite deposit, see Bárdossy, 1982) in Italy are formed by erosion of Cretaceous bauxite deposit (Mongelli et al., 2015). Previous studies on Italian bauxite deposits concentrated in ore deposit (Mindszenty et al., 1995), mineralogy (MacLean et al., 1997; Mameli et al., 2007), and element geochemistry (Mameli et al., 2020; Mongelli et al., 2014; Mongelli et al., 2015, 2017,2021; Sinisi, 2018). These studies provide good constrains for the formation age of the Italian bauxite deposits (Aptian – Turonian), mineralogical component (boehmite, hematite, kalinite, anatase, etc.), leaching process and the enrichments of LREE and other critical raw materials (e.g., Co and Ni), and paleo-environmental conditions. Some studies discuss the provenance problem of Italian bauxite deposits by element geochemistry and a few zircon U-Pb ages. Different potential source rocks have been proposed: (1) Cretaceous debris and in situ marly layer (MacLean et al., 1997); (2) alluvial sheets derived from the already weathered Variscan basement that hosts a few mafic rocks (Mameli et al., 2007, 2020); (3) weathering materials from continental margin of North Africa (Mongelli et al., 2016; Sinisi, 2018) and (4) the Dinaric and Carpatho-Balkan orogenic belts with its Cretaceous bimodal volcanism (Boni et al., 2012). Thus, the parental affinities problem of the Italian bauxite deposits is still in debate and a systemic study is necessary.

In this study, we provide new and systemic detrital zircon U-Pb ages and Hf isotope data from the representative Cretaceous bauxite deposits in the Sardinia and Adria regions of southern Italy. Combining isotopic constraints with the published geochemical data our study reveals the provenance difference between the Sardinia~~n~~ and Adria bauxite deposits further improving our knowledge on the paleogeography and the tectonic evolution of the Alpine Tethys.

2. Geological background

Bauxite deposits in Italy are concentrated in the present Sardinia Island, central-southern Apennines and Adria (Fig. 1A). These areas are located in the converging zone between the African and Eurasian plates since Cretaceous (Fig. 1B), with the complicated history of tectonic evolution (Dewey et al., 1989). Sardinia is a microplate, which before its drift in early Miocene time, was part of the southern margin of the European plate (Alvarez, 1972, Speranza et al., 2002). Adria, the foreland of the Apennines chain, is considered a single plate separated from the Africa plate by the Ionian basin, which is thought as a remnant of the recently questioned Mesogea (Channell et al., 2022) or as an abortive rift (Vitale et al., 2018).

Sardinia consists of a Variscan metamorphic basement intruded by Carboniferous-Early Permian granites capped by Mesozoic carbonate covers and Cenozoic mixed volcanic and sedimentary successions. The basement formed during the collision between Gondwana and Laurussia and the intervening terranes (Cappelli et al., 1991; Rossi et al., 2009; Cruciani et al., 2015). It includes Carboniferous, mostly magmatic rocks, Cambrian to Lower Carboniferous metasedimentary sequences, and large volumes of metavolcanic rocks, mainly Ordovician in age (Fig. 1C). All penetrative deformation structures, metamorphism (which increases from SW to NE Sardinia) were generated during the Variscan collision, whereas a large calc-alkaline magmatic activity was widely linked to the post-collisional evolution of this orogenic belt (Cortesogno et al., 1998; Casini et al., 2015; Secchi et al., 2022 and reference therein). Particularly, Late Variscan plutonic rocks are widespread in Sardinia and Corsica islands (Fig. 1C), where the "Corsica-Sardinia batholith" (Rossi and Cocherie, 1991), emplaced between 340 and 288 Ma (U-Pb ages on zircon; Cocherie et al., 2005; Casini et al., 2015). Pluton emplacement has been associated with a transitional context between shear-dominated transpression and post-orogenic crustal extension between Late Carboniferous and Early Permian (Gaggero et al., 2007; Casini et al., 2015; Secchi et al., 2022). During Mesozoic (Middle Triassic – early Cretaceous), > 1000-m-thick carbonate succession was deposited in Sardinia (Fig. 1C). The lower parts are Triassic dolostone, limestone and evaporite, which are overlain by > 500 m of Jurassic limestone and dolostone that grade into a regressive, 20-m-thick, greenish marlstone indicating the brackish environment. This marlstone is overlain by a ~ 300-meter-thick Lower Cretaceous (Barremian – Aptian) bioclastic grainstone formed in outer shelf environment. An Albian-Cenomanian stratigraphic hiatus is marked by different bauxite deposits (Fig. 2) (Combes et al., 1993; Combes and Bárdossy, 1996; MacLean et al., 1997; Mameli et al., 2007). The stratigraphic hiatus was caused by the emergence and karstification of the carbonate shelf (Mameli et al., 2020), which was caused by the far-field effect of the transpressional motion between the Iberian and European plates (Schreiber et al., 2011; Mameli et al., 2020).

Adria Plate and its interplaying terranes (e.g., Sardinia, Corsica, Iberian, Fig. 1B) went through similar tectonic pathway, they detached from the northern Gondwana margin during mid-Paleozoic, drifting north to become part of central Europe (Sirevaag et al., 2016). Bauxite deposits in Adria are found in the Apulia and the southern Apennines regions. During Mesozoic, the areas were part of the Adriatic margin of

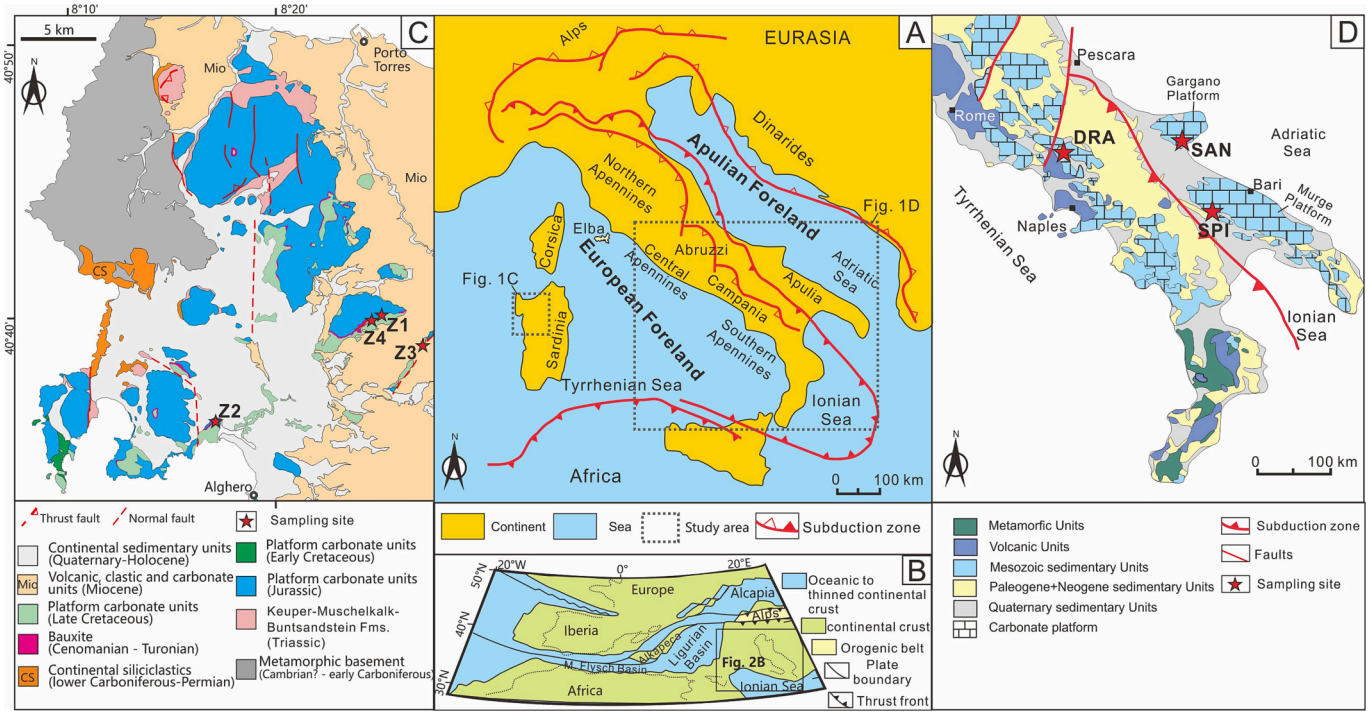

Fig. 1. (A) Simplified present-day tectonic sketch of the Italian peninsula and Sardinia-Corsica islands where the main subduction zones are shown; (B) Cretaceous paleogeography of Alpine Tethys and adjacent continental margins (modified from Handy et al., 2010); (C, D) Geological maps of Sardinia and central-southern Italy respectively, including localization of sampled bauxite ores.

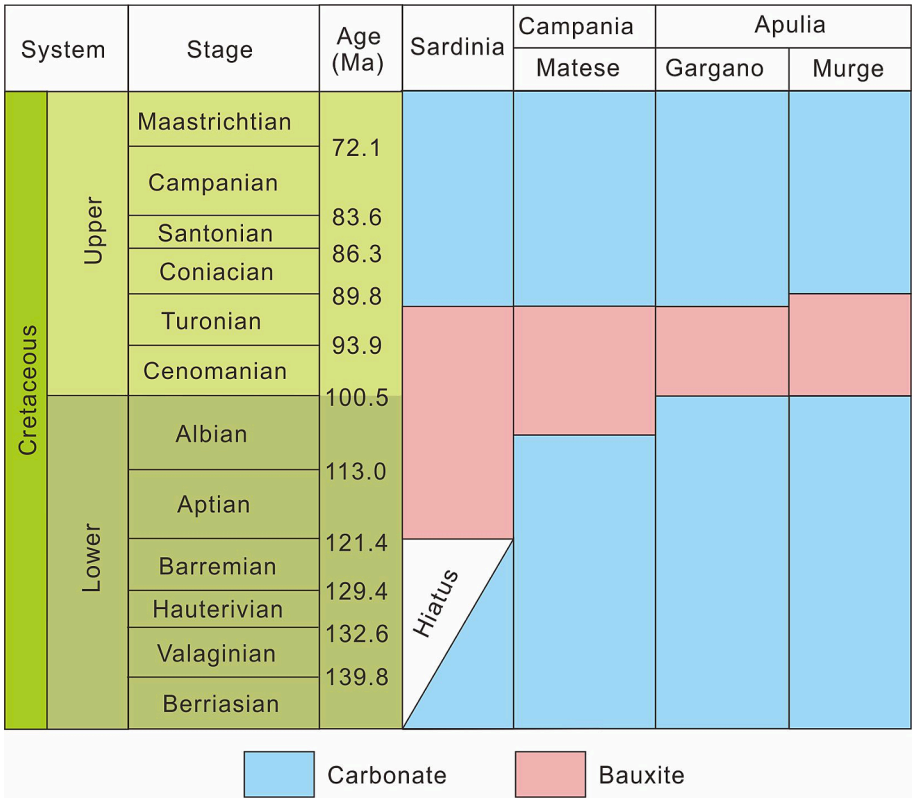

Fig. 2. Geochronological frame for the bauxite deposits in Sardinia and Adria, Italy, refer to Mongelli et al. (2017).

the Liguria-Piemonte segment of the Alpine Tethys (Mikes et al., 2008). The Apulia region extends for 350 km in southeast Italy between the Adriatic Sea and the Ionian Sea (Fig. 1A). From the Triassic to early Cretaceous, the Apulian Platform (AP) occurred in the passive continental margin (Vlahović et al., 2005). The AP mainly consists of metre-scale, shallowing-upward carbonates with aggradational cycles.

Carbonate deposition was frequently punctuated by ephemeral subaerial exposure (as indicated by palaeosols and palaeokarst) resulting from interactions of platform subsidence, long-term sea level change, and superimposed higher-order eustatic oscillations with the actual rate of carbonate production (Mindszenty et al., 1995). The southern Apennines is the NW-SE oriented southern segment of the Apennines thrust belt, either a crystalline basement wedge or the sedimentary cover exist in its deep (Scrocca et al., 2005). During Mesozoic, the obvious sedimentary differentiation showed in the Apennine area (Fig. 1D), including the carbonate platform in the southwest (probably remnants of a once larger single Apennine Carbonate Platform, ACP) and deeper basin in the southeast (Umbria-Marche in the northern and Lagonegro in the southern part of the chain, Boni et al., 2012). Similar to Sardinia, the ACP was punctuated by repeated uplifts (Aptian-Albian stages, Fig. 2), locally testified by bauxite deposits.

3. Sampling

Totally-seven representative samples were collected from the main Cretaceous bauxite deposits of southern Italy; four samples (Z1 to Z4) came from NW Sardinia and three samples (DRA, Dragoni site, Campania District; SPI, Spinazzola site and SAN, San Giovanni Rotondo site, Apulia District) were acquired from Adria (Fig. 3).

The samples from Sardinia were collected in deposits of different types according to the classification of Mameli et al. (2007). Z1 and Z2 samples came from a type 2 bauxite deposit, which lays on weakly karstified dolomitic limestone of Jurassic age in proximity of the Alghero airport. Z2 sample was representative of red bauxite layer generally located at the bottom of the section and Z1 sample was representative of the bleached part of same deposit. Z3 sample is representative of type 1 deposit, which lays on the marly beds and is representative of the intermediate part of the section, generally enriched in residual minerals. Z4 sample was picked near the city of Sassari in a mine that produced about 3 million tons of mineral, almost completely through an underground plant at Olmedo village. This sample comes from a single, large pile of ore representative of the four types of deposits. For each deposit 20 kg of ore were obtained by means of mass and channel sampling, which in turn were ground and reduced by crusher.

As for the Adria samples, the Spinazzola and Dragoni ones were collected (about 25 kg) in the intermediate part of open pits, whereas the San Giovanni Rotondo sample (about 30 kg) was collected in the upper part of an abandoned mine site. At the Dragoni site the bauxite bodies form flat, contiguous lenses of a few meters in thickness overlying the Upper Cretaceous karstified bedrock and covering the transition between Albian and Cenomanian. In the Spinazzola sampling site, the bauxite deposit is 20 m-thick and preserves both the Valanginian–Cenomanian carbonate footwall (*Calcare di Bari Formation*) and the transgressive, shallow-water Coniacian–Campanian limestones (*Calcare di Altamura Formation*) at the hanging wall. The San Giovanni bauxite consists of the sedimentary infill of both canyon-like cavities and irregular 3–10-m-thick lenses lying between the karstified *San Giovanni Rotondo limestone* (Valanginian–Aptian) at the bottom, and the transgressive *Altamura limestone* (Coniacian– Santonian) at the top. Further information on the sampling sites can be found in Mongelli et al. (2014), Buccione et al. (2016), and Sinisi (2018), respectively.

4. Analytical techniques

4.1. Pretreatments

Zircon grains were separated by standard heavy liquid and magnetic separation techniques from seven samples. Zircon grains were selected and mounted in epoxy resin, polished and finally coated with gold. The internal texture of these grains was examined by cathodoluminescence (CL) imaging using a scanning electron microprobe at the China University of Geosciences (Wuhan).

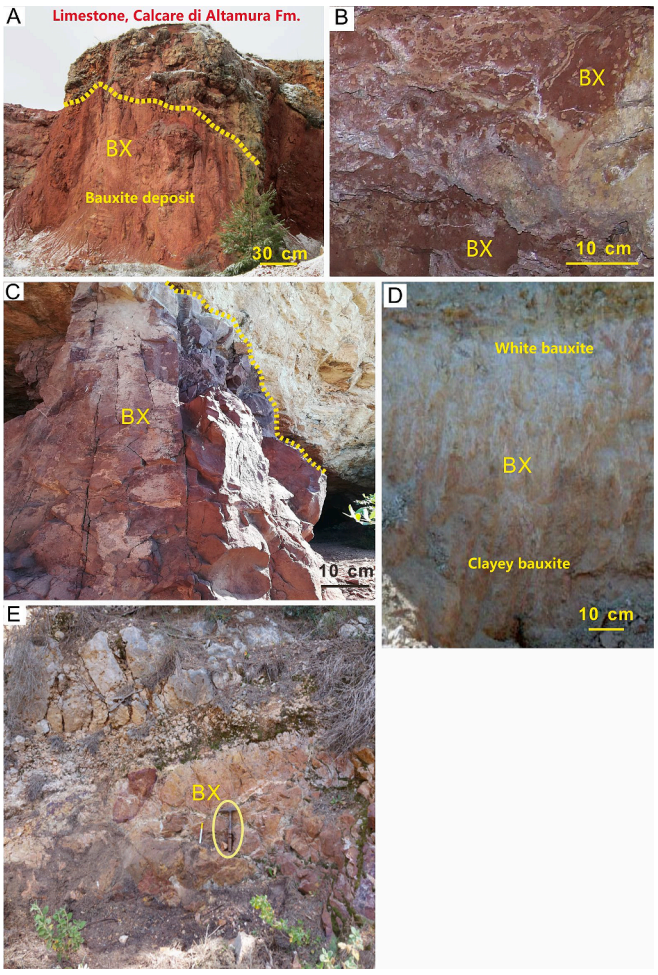

Fig. 3. Field photos for bauxite deposits of Sardinia and Adria: (A) Canyon-like bauxite deposit in Spinazzola, Murge; (B) Bauxite section in San Giovanni Rotondo, Gargano; (C) Bauxite section in quarry of Dragoni, Matese-Casertano; (D) Sardinian bauxite (Type 1 deposit at East of Olmedo) grading downward from white bauxite into clayey bauxite; (E) Sardinian bauxite (Type 2 at Monte Murone), the hammer in the yellow circle was used as the scale bar for this photo. Detail of description for bauxite deposits, please see (Boni et al., 2012; Mongelli et al., 2014, 2021). BX - Sampled bauxite position. (For interpretation of the references to colour in this figure legend, the reader is referred to the web version of this article.)

4.2. Zircon U-Pb age analyses

In situ zircon U-Th-Pb analyses was processed at the Sun Yat-sen University (SYSU, Zhuhai) by an iCAP-RQ-ICP-MS coupled with an ArF-193 nm GeolasHD laser-ablation system. A spot size of 32 μm with a laser repetition rate of 5 Hz was used for ablating zircons. Standard zircons Plešovice (337 ± 0.4 Ma) and 91,500 (1065 ± 5 Ma) were used as external calibration standards and ^{29}Si was used as the internal standard. Helium was used as the carrier gas to enhance the transport efficiency of the ablated material. Off-line raw data processing were carried out by the GLITTER program (Griffin et al., 2008), and the relevant statistics (e.g., age histograms, frequency curve fitting, and weighted averaged ages) were calculated using the Isoplot v4.15 program (Ludwig and Center, 2001). Zircon ages with a calculated discordance of < 10 % are considered to be valid.

4.3. Zircon Hf isotope analyses

Experiments of in situ Hf isotope ratio analysis were conducted using a Thermo Fisher Neptune Plus MC-ICP-MS in combination with a

Coherent Geolas HD excimer ArF laser ablation system at the Wuhan Sample Solution Analytical Technology Co., ltd, China. A "wire" signal smoothing device is included in this laser ablation system, by which smooth signals are produced even at very low laser repetition rates down to 1 Hz. Helium was used as the carrier gas within the ablation cell and was merged with argon (makeup gas) after the ablation cell. Small amounts of nitrogen were added to the argon makeup gas flow for the improvement of sensitivity of Hf isotopes. Compared to the standard arrangement, the addition of nitrogen in combination with the use of the newly designed X skimmer cone and Jet sample cone in Neptune Plus improved the signal intensity of Hf, Yb and Lu by a factor of 5.3, 4.0 and 2.4, respectively. All data were acquired on zircon in single spot ablation mode at a spot size of 44 μm. The energy density of laser ablation that was used in this study was ~ 7.0 J cm^{-2}. Each measurement consisted of 20 s of acquisition of the background signal followed by 50 s of ablation signal acquisition. Detailed operating conditions for the laser ablation system and the MC-ICP-MS instrument and analytical method are the same as description by Hu et al. (2012). Off-line selection and integration of analyte signals, and mass bias calibrations were performed using ICPMSDataCal.

5. Results

5.1. Zircon morphology

Cathodoluminescence (CL) images of the detrital zircon grains reveal a diverse suite of sizes and internal structures (Fig. 4), including three main types of zircon group: (1) euhedral-subhedral zircon grains with well-developed oscillatory zoning and lengths of long axis are 83–200 μm, indicating a magma or large melt reservoir origin; (2) subhedral-subrounded grains contain a homogeneous or oscillatory zoned core surrounded by a magmatic mantle that is oscillatory zoned and/or a bright metamorphic rim lacking internal structure, indicting multiple phases of growth or recrystallization (3) sub-rounded to rounded zircon grains with partial oscillatory or homogeneous bright/dark zones, indicating recrystallization.

5.2. Detrital zircon U-Pb ages

A total of 427 zircon analyses were undertaken from seven bauxite ore samples. Discussion of age data is based on $^{207}Pb/^{206}Pb$ and $^{206}Pb/^{238}U$ apparent ages for the older (>1000 Ma) and younger (<1000 Ma) zircon grains, respectively. For detailed zircon U–Pb isotopic compositions, please check Supplementary Data (Table S1). All analyses are shown on Concordia plots (Fig. 5). About 87.5 % (374 out of 427) analyses have fallen on or near Concordia (discordance ≤ 10 %) and are also displayed on relative probability plots and age histograms by the software Isoplot v4.15 (Fig. 6). Uncertainties on individual analyses in the data table and Concordia plots are all presented at 1σ.

5.2.1. Z1 –Monte Murone, Sardinia

Three grains from sample Z1 are older than 2000 Ma with the oldest yielding an age of 2440 ± 39 Ma. Four analyses are distributed between 1031 and 1832 Ma without any age peak. Two groups of analyses can be distinguished in the interval 700 and 915 Ma, with average ages of 896 ± 36 Ma (MSWD = 1.2, n = 4) and 731 ± 45 Ma (MSWD = 2.8, n = 4). Most analyses are scattered between 640 and 273 Ma, with the dominant age peak of 454.4 ± 5.8 Ma (MSWD = 2.3, n = 34), and two subdominant age peaks at 582 ± 16 Ma (MSWD = 4.4, n = 14) and 292 ± 8 Ma (MSWD = 1.7, n = 8) (Fig. 6A).

5.2.1.1. Z2 –Monte Murone, Sardinia. The oldest analyzed grain in this sample is 2799 ± 42 Ma. Four analyses yielded ages in the interval of 798 Ma to 1642 Ma. Analysis of 10 grains in the range of 605 Ma to 708 Ma with an average age of 637 ± 28 Ma (MSWD = 6.2). A further group of five analyses gives a weighted mean age of 565 ± 31 Ma (MSWD = 3.1). The main age cluster occurs in the range of 429 – 503 Ma with an average age of 456 ± 5 Ma (MSWD = 1.7, n = 47). The youngest age cluster in this sample occurs at 291 ± 19 Ma (MSWD = 2.5, n = 4) (Fig. 6B).

5.2.1.2. Z3 – Olmedo, Sardinia. Analyzed grains from sample Z3 range in age from 2953 to 112 Ma (Fig. 6C). Three grains give Archean to Paleoproterozoic ages. Six grains yield ages from 1387 Ma to 733 Ma without any age peak. Analysis of 14 grains is in the range of 608 – 682 Ma with two age groups at 639 ± 19 Ma (MSWD = 2.8, n = 10) and = 541 ± 32 (MSWD = 2.2, n = 4). The main age peak shows in 458 ± 6 Ma (MSWD = 2.0, n = 38). Analyses between 285 and 398 Ma have two distinct age clusters, one with ages between 326 and 258 Ma (335 ± 23 Ma, MSWD = 2.7, n = 4) and one with ages distributed between 285 and 308 Ma forming a peak at 295 ± 11 Ma (MSWD = 1.4, n = 5). The youngest grain (Z3-21) in this sample gives the age of 112 ± 3 Ma.

5.2.1.3. Z4 – Olmedo Mine, Sardinia. One analyzed grain from Z4 sample shows the Paleoproterozoic age of 2580 ± 37 Ma. Eight analyses scatter in age range from 2058 Ma to 754 Ma, showing no obvious age peak. Eighteen analyses are distributed between 678 Ma and 518 Ma, consisting one wide age peak at 585 ± 22 Ma (MSWD = 8.9, n = 18). In the range from 410 to 510 Ma, a distinct age peak occurs at 466 ± 9 Ma (MSWD = 4.3, n = 34). A further 19 grains have ages distributed between 321 and 278 Ma, giving an age of 294 ± 7 Ma (MSWD = 3.8) (Fig. 6D).

5.2.1.4. DRA – Dragoni, Matese. The oldest analyzed grain from the DRA sample is concordant with an age of 2369 ± 39 Ma. Nine analyses are distributed in the range of 440 Ma to 1069 Ma, with some Pre-Mesozoic minor age peaks at ~ 447 Ma, ~532 Ma and ~ 617 Ma. Two distinct age clusters are presented in the range of 100 – 200 Ma with 177 ± 10 Ma (MSWD = 3.2, n = 4) and 136 ± 5 Ma (MSWD = 5.5, n = 6) (Fig. 6E).

5.2.1.5. SPI – Spinazzola, Murge. Three slightly discordant analyses (94 % – 95 %) have ages of 2544 Ma, 2550 Ma and 2725 Ma (Fig. 6F). Five analyses distribute in the broad range from Mesoproterozoic to Paleozoic (301 Ma to 1316 Ma). Seven analyses give the Jurassic age range 184 Ma – 165 Ma, with the average age of 176 ± 10 Ma (MSWD = 9.3).

5.2.1.6. SAN – San Giovanni Rotondo, Gargano. Zircon grains from sample SAN range in age from 3086 Ma to 93 Ma (Fig. 6G). This sample gives different zircon age pattern comparing to other samples. Including following features: (1) without obvious age peak, minor age peaks occur in ~ 450 Ma, ~2000 Ma and ~ 2500 Ma; (2) the oldest zircon is acquired the age of 3086 ± 31 Ma, older than all other samples (2900 – 2400 Ma); (3) two Early Cretaceous aged zircon (93 Ma and 100 Ma) are shown in this sample.

5.3. Zircon trace elements

The geochemical compositions for 370 zircon grains (for those discordance ≤ 10 %) are presented in Supplementary Materials (Table S2). Th/U ratios of analyses are in the range of 0.007 – 2.074. Zircon with lower Th/U rations (<0.1) are generally with Pre-Mesozoic ages (317 – 1387 Ma), all of them come from samples of Sardinia. Series ratios of U/Yb (0.075 – 38.182), Nb/Yb (0.001 – 0.119), Hf/Th (1.051 – 2679.568) and Th/Nb (3.332 – 462.592) are also calculated for analyses.

5.4. Zircon Lu-Hf isotope results

The Lu-Hf isotopic compositions for 86 grains with ages ranging from

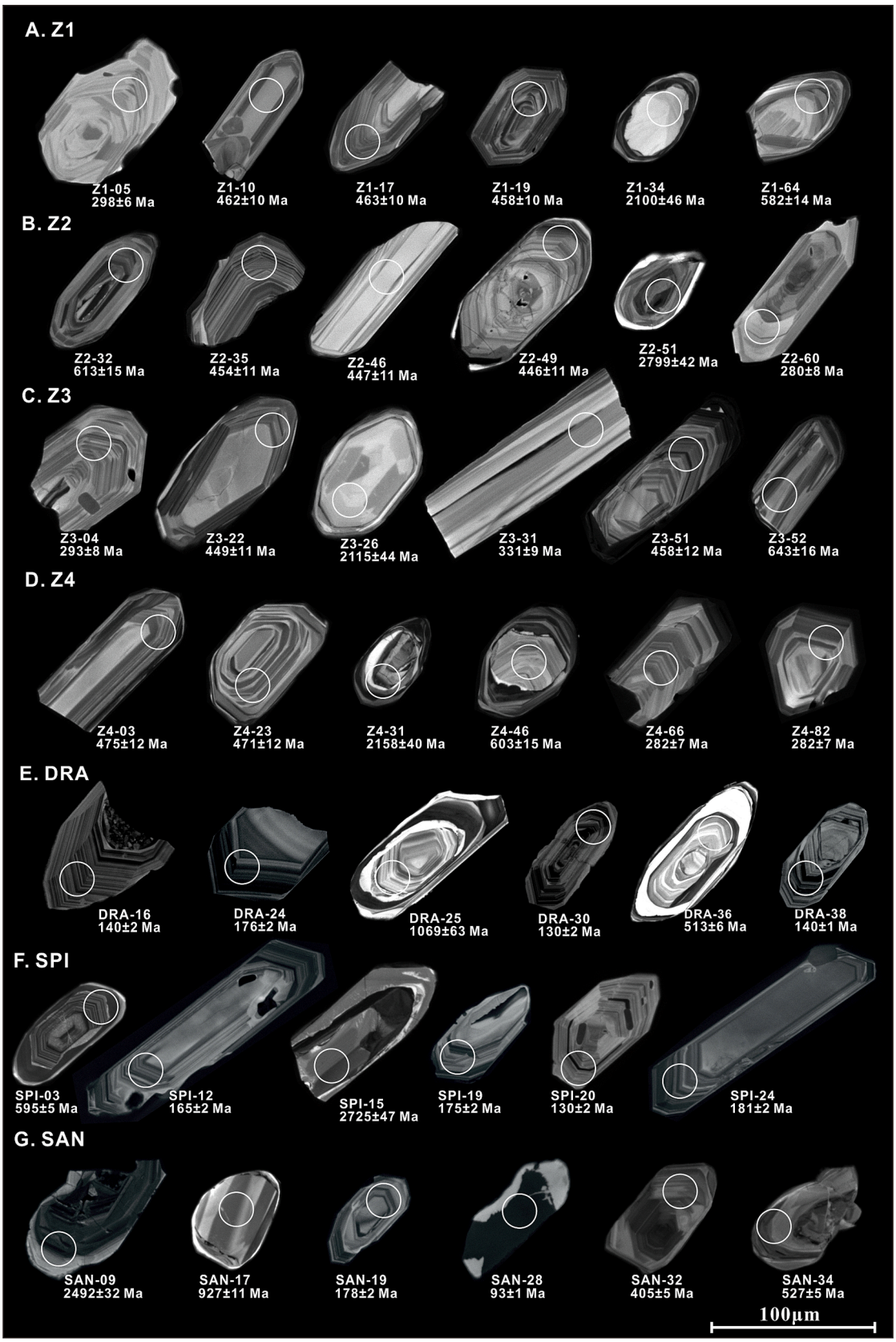

Fig. 4. Cathodoluminescence (CL) images showing internal structures of representative zircons from A-D are bauxite deposits samples (Z1 to Z4) of Sardinia; E-G are bauxite deposits samples (DRA, SPI, SAN) of Adria.

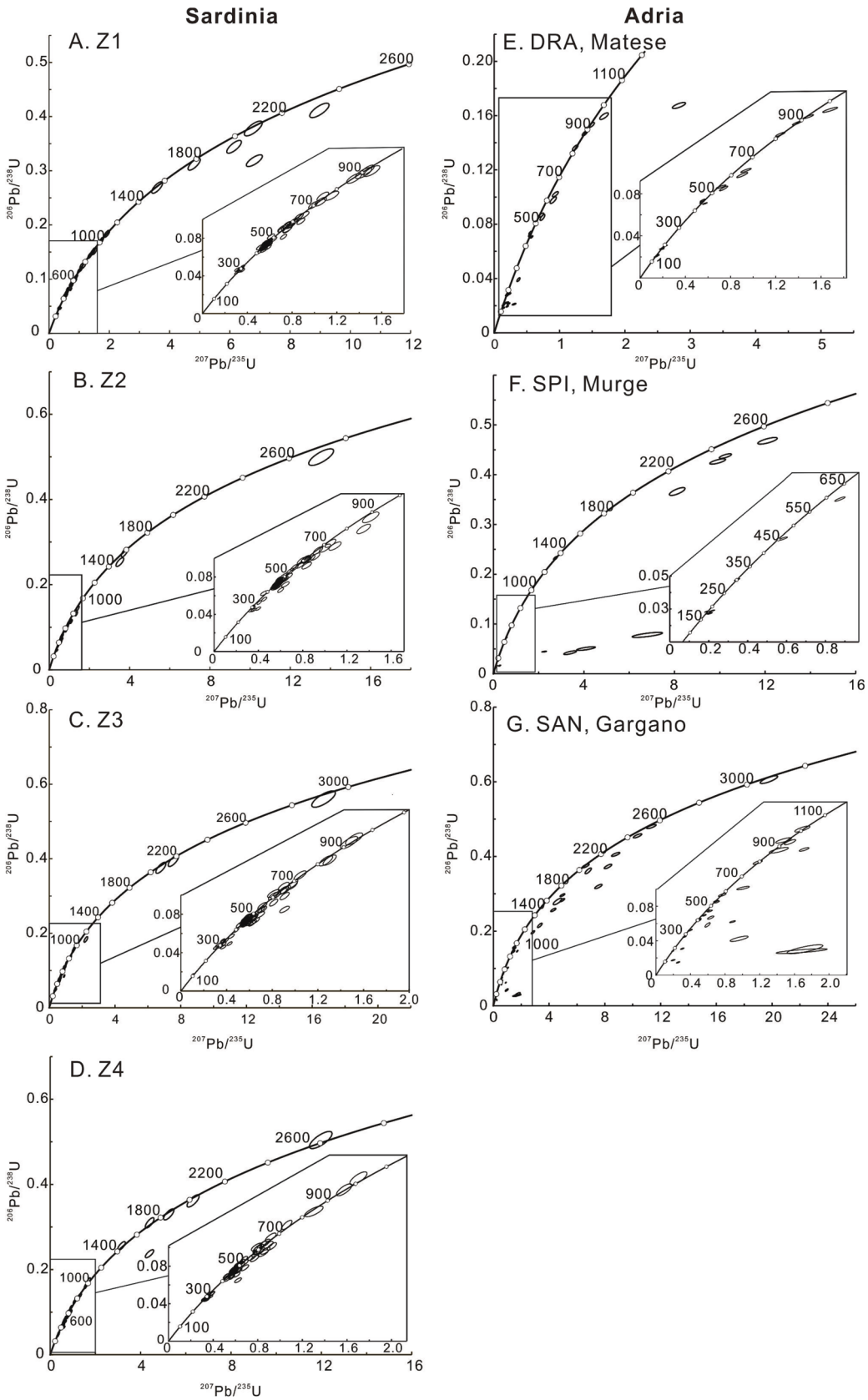

Fig. 5. Detrital zircon U-Pb Concordia diagrams of bauxite deposits samples (Z1 to Z4) of Sardinia (A-D); bauxite deposits samples (DRA, SPI, SAN) of Adria (E-G).

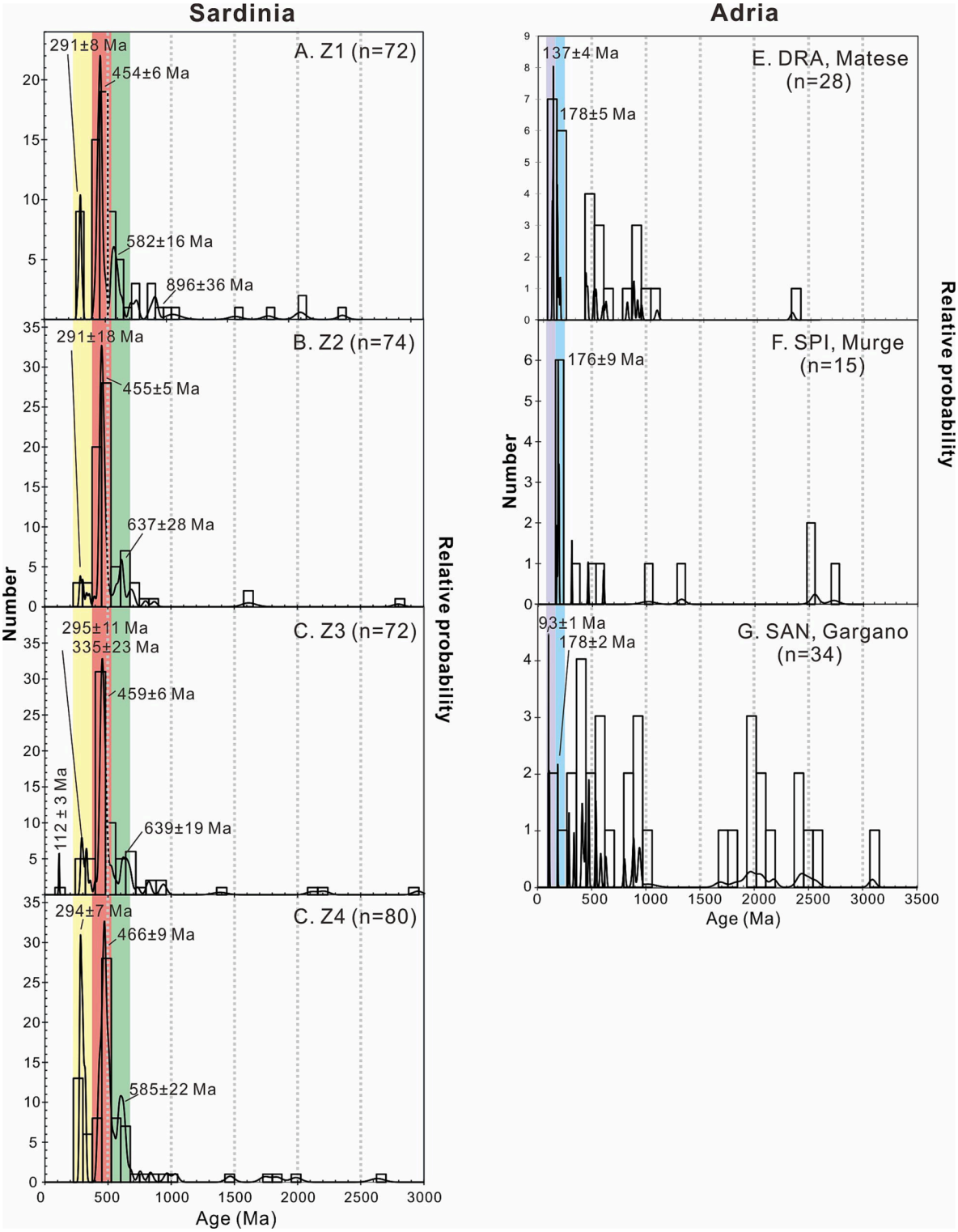

Fig. 6. Age histogram and relative probability plots from bauxite deposits samples (Z1 to Z4) of Sardinia (A-D); bauxite deposits samples (DRA, SPI, SAN) of Adria (E-G).

130 Ma to 618 Ma are presented in Supplementary Materials (Table S3). Zircon grains from Sardinia bauxite deposits display initial $^{176}Hf/^{177}Hf$ ratios of 0.282304 to 0.282696, corresponding to $\varepsilon_{Hf}(t)$ values of −5.7 to + 9.6 (Fig. 7). For zircon grains from Adria, they have similar initial $^{176}Hf/^{177}Hf$ ratios (0.282298 – 0.282612), but lower $\varepsilon_{Hf}(t)$ values (-13.8 to + 2.6).

A decreasing $\varepsilon_{Hf}(t)$ trending matches with decreasing zircon ages (Fig. 7). Zircon grains with age of 618 – 527 Ma give $\varepsilon_{Hf}(t)$ values in the range of −4.31 to + 9.61 with the average of + 1.35 ± 4.46 ($n = 7$), Hf model ages (T_{DM2}) ranging from 0.9 Ga to 1.6 Ga. Aging 480 – 405 Ma zircon grains contain $\varepsilon_{Hf}(t)$ values between −5.66 to + 6.43, with the average of −2.00 ± 1.97 ($n = 55$), T_{DM2} = 0.9 Ga – 1.5 Ga. For younger zircon grains (302 – 278 Ma), there is no positive $\varepsilon_{Hf}(t)$ value, ranging from −0.65 to −3.23, with the average of −1.61 ± 0.96 ($n = 10$), T_{DM2}

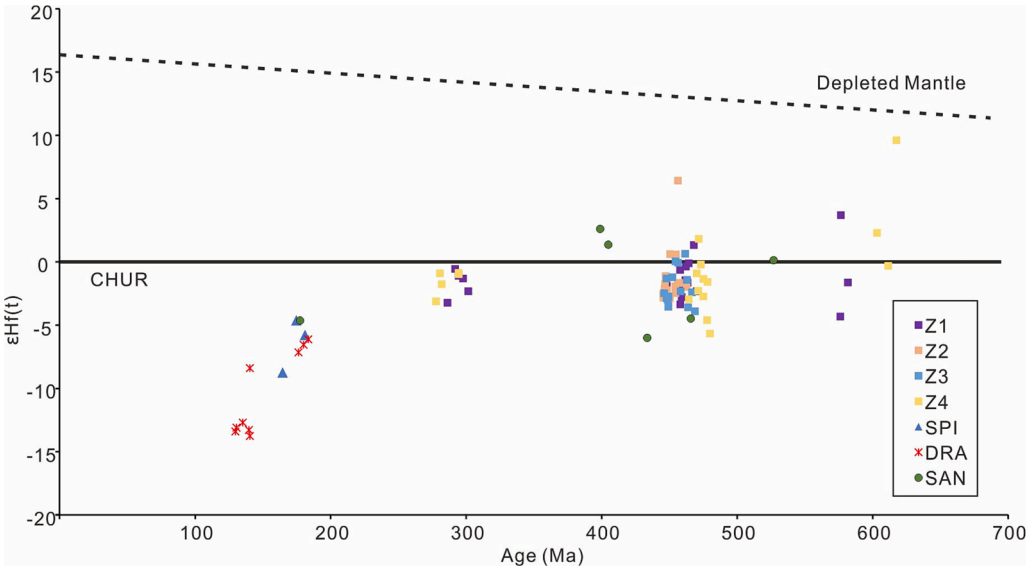

Fig. 7. Diagram of εHf(t) values versus ages of zircon grains for bauxite deposits samples (Z1 to Z4) from Sardinia (Z1 to Z4) and Adria (DRA, SPI, SAN).

= 1.2 Ga – 1.4 Ga. The youngest zircon cluster (130 – 183 Ma) contains the most negative $\varepsilon_{Hf}(t)$ values (-4.61 to −13.75, with the average of −9.09 ± 3.62, $n = 13$), T_{DM2} = 1.3 Ga – 1.8 Ga.

6. Discussions

6.1. Zircon genesis

Most valid (discordance ≤ 10 %) zircon grains acquired from this study indicate a magmatic origin (357 out of 374 grains), while seventeen grains indicate the metamorphous origin with age in the 317 – 1387 Ma range. This statement is supported by the following evidences: (1) in CL images, magmatic zircon shows internal oscillatory zoning, metamorphic zircon shows homogenous internal structure (Corfu et al., 2003); (2) Th/U ratios of magmatic zircon are > 0.1, whereas those of metamorphic zircon are < 0.1 (Fig. 8A) (Rubatto, 2002).

The distribution of selected trace element in zircon grains has been applied to distinguish their tectonic settings (Hawkesworth and Kemp, 2006). All analyses were plotted on the Nb/Yb – U/Yb diagram to examine the original crystallized places of zircon (magmatic arc vs mantle, Grimes et al., 2015). Most zircon grains fall in the field of magmatic arc, indicating the dominant continental arc sources, whereas only eleven zircon grains plot in the mantle field (Fig. 8B). In order to constrain the tectonic settings where zircon formed, the Th/Nb – Hf/Th diagram plot was produced (Yang et al., 2012). This plot was built by the different activities of high field-strength elements in the zircon grain to estimate the origin of them (Yang et al., 2012). In this diagram (Fig. 8C), the most of zircon grains fall in the arc-related/orogenic area, and only a small number of zircon are in the within-plate/anorogenic area.

Examination of Hf isotope results further indicate the source differentiation of zircon with various ages (Fig. 7). Late Neoproterozoic zircon (618 Ma – 576 Ma) with relatively positive $\varepsilon_{Hf}(t)$ values formed in juvenile materials. Late Cambrian to Early Devonian zircons (480 – 405 Ma) show large variation in $\varepsilon_{Hf}(t)$ values (-5.66 to + 6.43), suggesting reworking of older crustal components and involvement of juvenile material during magma generation. Both Late Carboniferous – Early Permian and Early Jurassic – Early Cretaceous zircon grains only contain negative $\varepsilon_{Hf}(t)$ values, indicating that they formed in the magma due to reworking of older crustal components.

6.2. Various provenances for Cretaceous bauxite deposits in the Sardinia and Adria regions

6.2.1. Variscan provenance of Turonian bauxite in Sardinia

In SW Sardinia, Cretaceous bauxite deposits unconformably overlies various rocks, including Upper Jurassic/Lower Cretaceous pure limestone, dolostone, and minor marlstone. Previous studies proposed two potential parental affinities for these bauxite deposits based on geochemical affinity: (1) the debris plus a thin marly horizon that occurs only in places limestone (MacLean et al., 1997) and (2) alluvial sheets from metamorphic basement (Mameli et al., 2020). Our new evidences indicate that Cretaceous bauxite deposits of SW Sardinia have been derived from the same source rock(s): (1) four samples from different sites show very similar geochronological pattern (Fig. 6A-D); (2) multi-dimensional scaling of Sardinian samples concentrated in the small area (Fig. 9A); (3) samples share the similar pattern in the depositional lag time diagram (Fig. 9B). At least three distinct age peaks can be observed, from young to old are: (1) Early Permian (291 – 295 Ma), (2) Middle – Late Ordovician (454 – 465 Ma), and (3) Late Neoproterozoic (582 – 639 Ma). Some minor age peaks (only containing one to three zircon grains) can also be found in all four samples, including Early Neoproterozoic (800 – 900 Ma), Neoproterozoic – Mesoproterozoic (900 – 1100 Ma) and Paleoproterozoic to Mesoarchean ages. Particularly, the youngest zircon was discovered in the Z3 sample, giving the age of 112 ± 3 Ma (Aptian – Albian).

Zircon age spectra, trace element and Hf isotope in the Sardinian bauxite deposit record a completed tectonic history of the Sardinia microplate (see Section 6.4). The singular Aptian – Albian zircon provides the maximum depositional age for the Sardinian bauxite deposit. This age is consistent with the previous stratigraphic constrain for this bauxite deposit (Mameli et al., 2007). Morphological (euhedral prism with well-developed oscillatory zone) and trace element (falling into the arc-related and magmatic arc zones) indicate that Sardinian bauxite deposit was produced by activities of the Early Cretaceous volcanic arc during evolution of the Neotethys.

The zircon cluster concentrated in the Late Carboniferous – Middle Permian age (340 – 270 Ma) corresponds to the final stage of the Variscan orogenic cycle (Casini et al., 2015; Paoli et al., 2017). Late Variscan Corsica–Sardinia Batholith (340 – 280 Ma) is considered to develop along the crustal shear zones between the northern Gondwana and central Europe (Casini et al., 2015). Magmatism of Early – Middle Permian age (270 – 290 Ma) in Sardinia and the southern Alps is

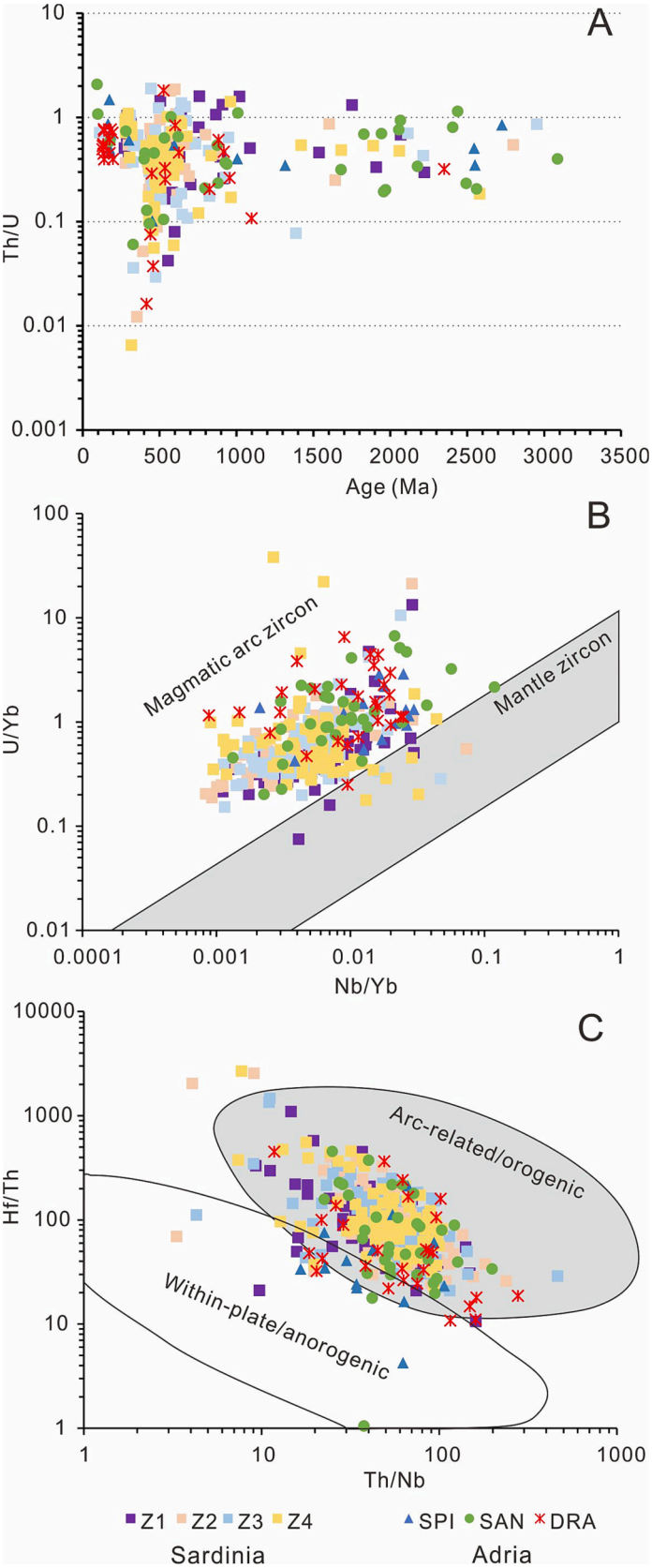

Fig. 8. Diagrams of (A) Th/U values versus ages, (B) Nb/Yb versus U/Yb (Grimes et al., 2015) and (C) Th/Nb versus Hf/Th of analyzed zircon (Yang et al., 2012) of analyzed zircon.

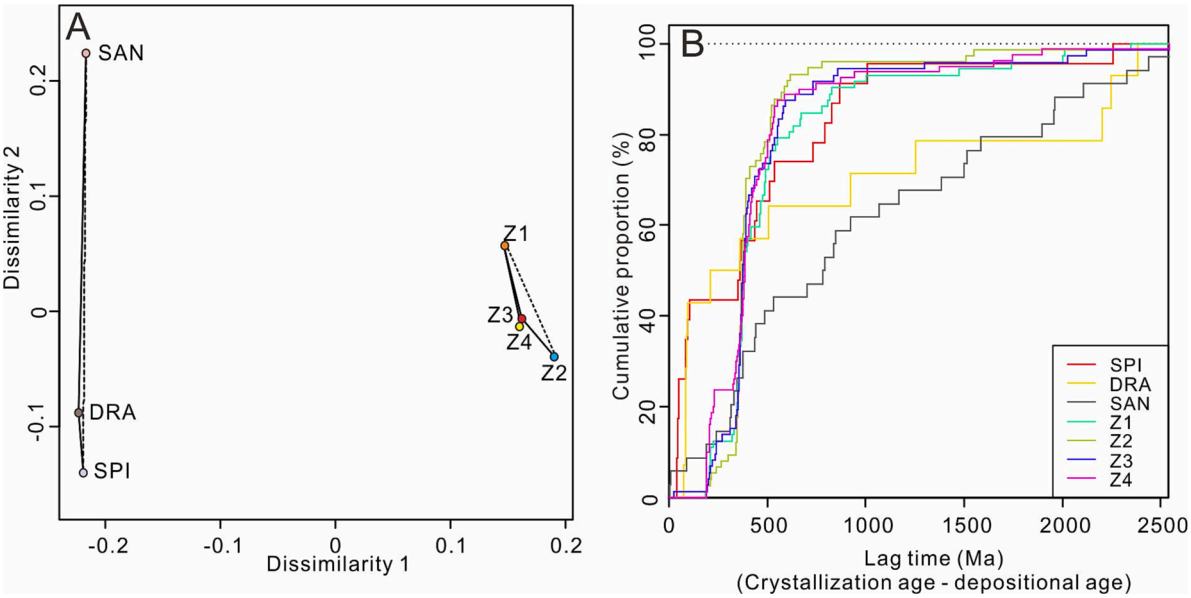

Fig. 9. (A) Multi-dimensional scaling and (B) "Depositional lag time" (depositional lag time = crystallization age minus depositional age) plots (Cawood et al., 2012) of analyzed zircon from Sardinia (Z1 to Z4) and Adria (DRA, SPI, SAN).

considered to represent the geodynamic transition from the subduction of Paleotethys to the opening of Neotethys (Cortesogno et al., 1998; Gaggero et al., 2007; Gretter et al., 2013; von Raumer et al., 2013). All of these zircons are in the magmatic arc/arc-related zone and their εHf(t) values are < 0, indicating the crustal affinity.

A large number of zircon analyses are in the age range of Furongian – Pridoli (490 – 420 Ma) with the age peak at 454 – 465 Ma, indicating a diachronous magmatism during this period in concomitance with the "Sardic phase" (Cocco and Funedda, 2017; Álvaro et al., 2020). Records of a series of magmatic events are widely discovered in Sardinia (Oggiano et al., 2010) and its adjacent areas (e.g., Tuscany, Elba Island, Central Iberia) (Montes et al., 2010; Paoli et al., 2017; Sirevaag et al., 2016). Oggiano et al. (2010) further divided three main volcanic events in Sardinia during Early Paleozoic: (1) intermediate and felsic volcanism (ca. 490 – 470 Ma), formed in the Cambro–Ordovician volcanic passive margin; (2) calc-alkalic rhyodacites (ca. 465 Ma), related to bimodal Mid-Ordovician arc volcanism during the Rheic ocean subduction; (3) alkalic metaepiclastites (ca. 440 Ma), due to rifting and collapse of the Mid-Ordovician volcanic arc. Hf isotope results from the Sardinian bauxite deposits show the major negative values and minor positive values, indicating the mixture of crustal and mantle sources. These results are consistent with element discrimination diagrams in which just few zircon grains are in the mantle and within-plate/anorogenic fields. Some metamorphic zircon grains also concentrate in this age range (Th/U < 0.1 and homogeneous internal structure), probably due to the Variscan metamorphism. Based on the evidences above, we believe Early Paleozoic zircons in our samples are related to subduction of the Rheic Ocean beneath northern Gondwana and the subsequent opening of the Paleotethys, as suggested by Arboit et al. (2019) and Paoli et al. (2017).

Further, also the continuous Cryogenian to Miaolingian (720 – 500 Ma) zircon age population largely documented along the European Variscan belt (Avigad et al., 2016; Ballèvre et al., 2001; Koglin et al., 2018; Žák and Sláma, 2018), is found in the Sardinian bauxite deposits. This age population is believed to link with Pan-African Event and represents Cadomian magmatic arcs of Late Neoproterozoic to Cambrian age accreted to the Gondwana margin (Azor et al., 2021; von Raumer et al., 2015). New zircon Hf isotope results from this age population, showing the average value of + 1.35 ± 4.46 ($n = 7$), are consistent with a main mantle source.

Sporadic zircon grains fall into the wide age distribution from Tonian to Mesoarchean (730 – 2950 Ma), with minor or no age peak. This part of old zircon age population has been discussed in previous studies on the Variscan, Apennine and Alpine basements, indicating the generation of zircon during breakup of Rodinia (860 – 750 Ma), the Grenville orogeny (ca. 1100–900 Ma) and some recycling zircon with Paleoproterozoic (ca. 2.2–1.6 Ga) and Paleoproterozoic–Mesoarchean age (ca. 2.9–2.4 Ga) (Arboit et al., 2019; Paoli et al., 2017). Cretaceous bauxite deposits inherit these old zircon grains from the underlying Variscan metasediments.

New zircon U-Pb geochronological and Hf isotope data revealed the similarity of the zircon age spectra from the Aptian – Albian bauxite deposits in Sardinia and Variscan metasediments, indicating the closed affinity between them. This statement is further supported by geochemical discrimination plot (Fig. 10), in which Sardinian bauxite deposit samples are closed to the sedimentary clastic rocks (representing by PAAS and cratonic sandstone).

6.2.2. *Mixed provenances for Albian – Turonian bauxite deposits in Adria*

Zircon age spectra in the Adrian bauxite deposits show obvious difference with the Sardinian bauxite deposits, indicating different parental affinities among the bauxite deposits from the two areas. Among the Adrian bauxite deposits, different locations also show some minor variations in zircon age distribution.

Bauxite deposits in Matese (central-southern Apennine, sample DRA) and Murge (Apulia, sample SPI) show similarity in the zircon age spectra. Although there are limited zircon analyses in two samples, a dominated age peak in Early Jurassic can be observed (176 – 178 Ma). A younger age peak at ca. 137 Ma is presented in bauxite deposit of Matese. Some minor age peaks are scattering at 440 – 460 Ma, 510 – 540 Ma, 900 – 1200 Ma and 2300 – 2600 Ma. For the SAN sample from Gargano, two youngest zircon grains (93 Ma and 100 Ma) constrain the Cenomanian as the maximum sedimentation age for this bauxite deposit. One Early Jurassic zircon grain (178 Ma) suggests affinity between SAN sample and other two samples in Adria region. However, the majority of zircon population shows close similarity with the Variscan basements at the ~ 450 Ma, ~2000 Ma, and ~ 2500 Ma age peaks coupled with series of zircon grains scattered in 520 – 1800 Ma.

Previous studies acquired limited detrital zircon age data from the Adrian bauxite deposit (Boni et al., 2012; Mongelli et al., 2016). Based

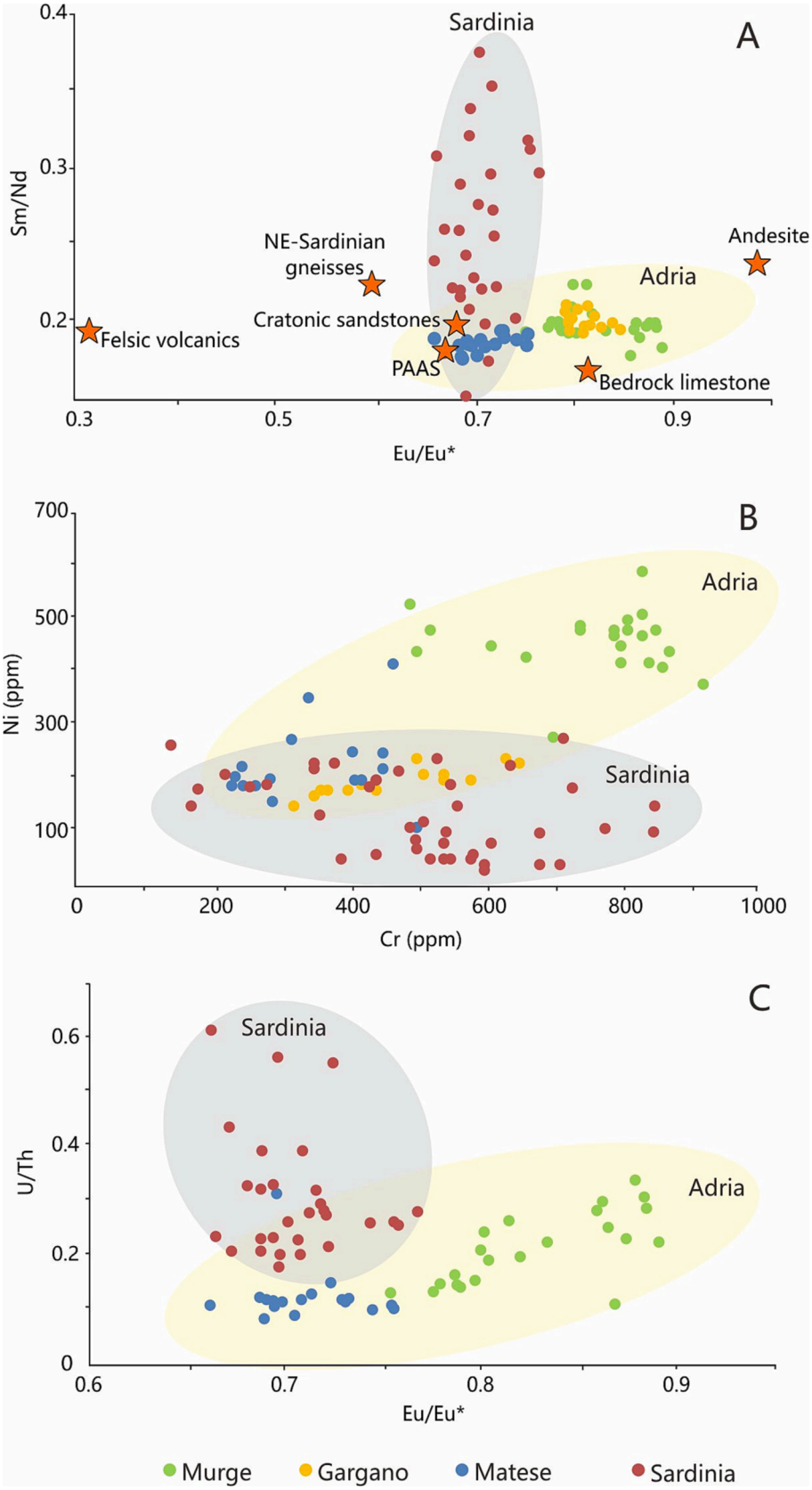

Fig. 10. Geochemical discrimination plots of (A) Sm/Nd versus Eu/Eu*; (B) Ni (ppm) versus Cr (ppm) and (C) U/Th versus Eu/Eu* of bauxite samples from Adria (n = 75) and Sardinia (n = 41). Data from (Boni et al., 2012; Mongelli et al., 2014, 2016, 2021; Mameli et al., 2007, 2020).

on 15 zircon grains from Matese bauxite deposit (Boni et al., 2012) and 12 zircon grains from the Otranto bauxite deposit (Mongelli et al., 2016), Early – Late Cretaceous age cluster (90 – 127 Ma) was shown in both deposits, with some minor age clusters in Late Paleozoic (300 – 315 Ma), Neoproterozoic (564 – 997 Ma) and Mesoproterozoic to Neoarchean (1542 – 2681 Ma). It is noteworthy that zircon age spectra were not the same in previous studies on bauxite deposits in Adria region compared with the results of this study. Some important differences include: (1) Early – Late Cretaceous ages wider in this study (93 – 137 Ma) than previously reported (90 – 127 Ma); (2) an Early Jurassic age peak (176 – 178 Ma) found in this study but absent in previous studies; (3) Pre-Mesozoic zircon found in all Adrian samples, but showing different age distribution, e.g., 622 – 697 Ma in Mongelli et al. (2016), 300 – 301 Ma in Boni et al. (2012), and ~ 450 Ma in our samples. The variation of zircon age populations in different studies may depend on both scarcity of valid zircon analyses leading to incomplete provenance information (Vermeesch, 2004) and differences in the parent rocks during the formation of bauxite deposits in different sites of Adria region. The latter explanation, however, might be supported by geochronological statistic and geochemical evidences. In geochemical discrimination diagram, dispersal of Adrian samples was relatively concentrated (Fig. 10). Early – Late Cretaceous and Early Jurassic age peaks were observed in all three samples in this study, multi-dimensional scaling of SAN, DRA and SPI samples indicates that they have connections in the source rock(s), although the SAN sample could have minor parental diversity with respect to the other two samples (Fig. 9A).

To sum up, the zircon age population in Adria, from published data and this study ($n = 99$), includes several main age clusters (Early – Late Cretaceous, Early Jurassic, Early Permian and Early – Middle Ordovician), significant in order to assess parental affinities (Fig. 11C). The maximum deposition age for the Adria bauxite deposit is Early – Upper Cretaceous and previous studies suggested a windborne source of volcanic activities from adjacent areas (Boni et al., 2012; Mongelli et al., 2016). During Cretaceous, evolution of Neotethys led to complex tectonic structures in southern Apennines and its surrounding areas (Patacca and Scandone, 2007). Several tuff layers have been found within the Cretaceous carbonate deposits in the Adria region, but they did not transform to bauxite (Bernoulli et al., 2004). Two potential sources were proposed for the Cretaceous zircon grains in Adria bauxite deposits: (1) subduction-related intrusive and effusive magmatism in the Dinaric and Carpatho-Balkan Orogenic Belts and/or (2) converging zone between the Eurasia and Adria plates (Boni et al., 2012). Our new data provide support for these sources, and zircon trace element compositions show that Cretaceous zircon in the Adria bauxite deposits were sourced from arc-related magmatic activities. Negative εHf(t) (−13.75 to −8.38 with the mean of −12.43 ± 2.01) further reveal the crustal affinity of the Cretaceous magmatic activities (Fig. 12).

Pre-Cretaceous zircon grains in the Cretaceous bauxite deposits have two possible explanations: (1) inherited zircon in the magma chamber or (2) weathering materials transported by wind. Late – Early Jurassic age peak (176 – 178 Ma) was firstly found within the Adria bauxite deposits. During Early – Middle Jurassic, the Vardar Ocean (at the western end of the northern Neotethys, Stampfli and Borel, 2004) in the northeastern side of the Adria Plate had ceased the spreading process, and began the stage of NNE-trending subduction in the West Vardar oceanic plate (Scherreiks et al., 2010; Scherreiks and BouDagher-Fadel, 2021). The initial time of subduction was constrained to Toarcian – Bajocian (180 –

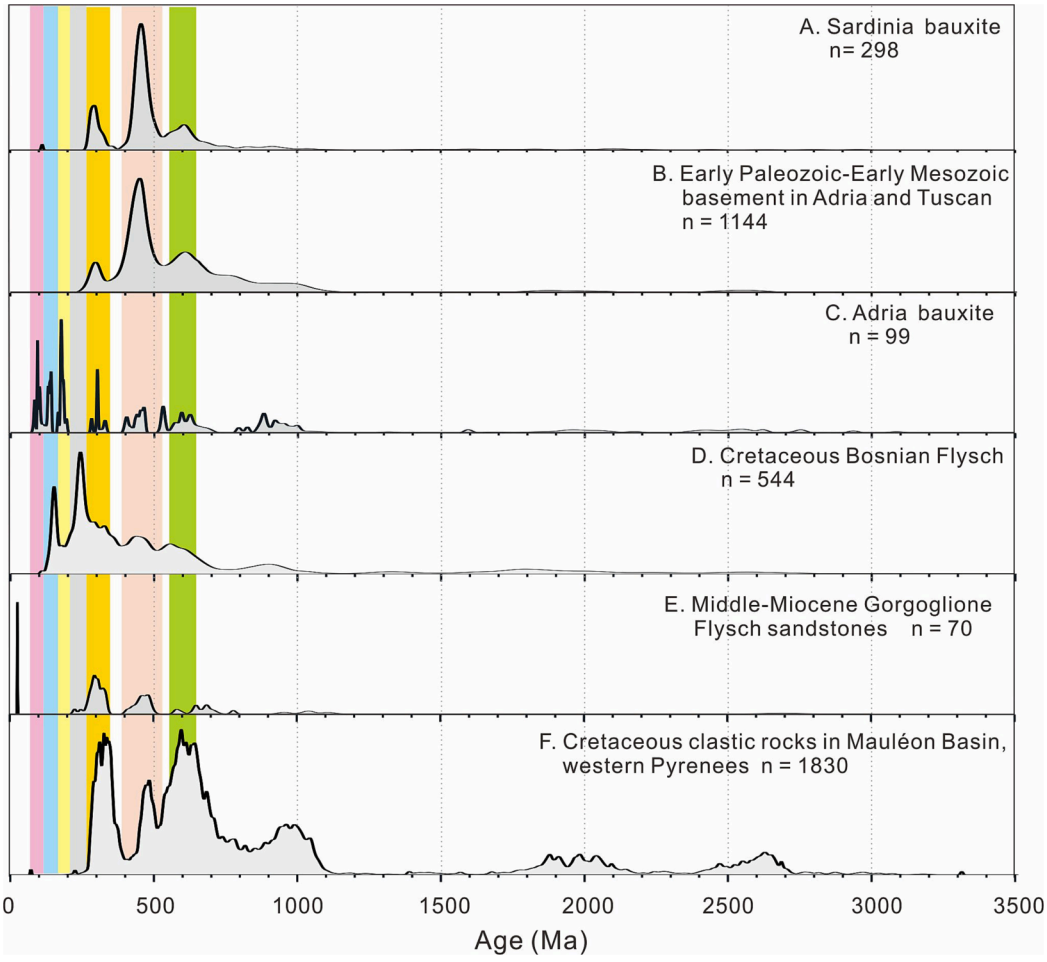

Fig. 11. Probability density plots of LA-ICPMS and fission track detrital zircon ages for (A) bauxite deposits in Sardinia; (B) Early Paleozoic – Early Mesozoic basement in Adria and Tuscan regions, data are from Sirevaag et al. (2016) and Paoli et al. (2017); (C) bauxite deposits in Adria, partial data are from Boni et al. (2012) and Mongelli et al. (2016); (D) Cretaceous Bosnian Flysch deposits from Mikes et al. (2008); (E) Middle Miocene Gorgoglione Flysch sandstone from Fornelli et al. (2020); (F) Cretaceous clastic rocks in Mauléon Basin, western Pyrenees from Hart et al. (2016).

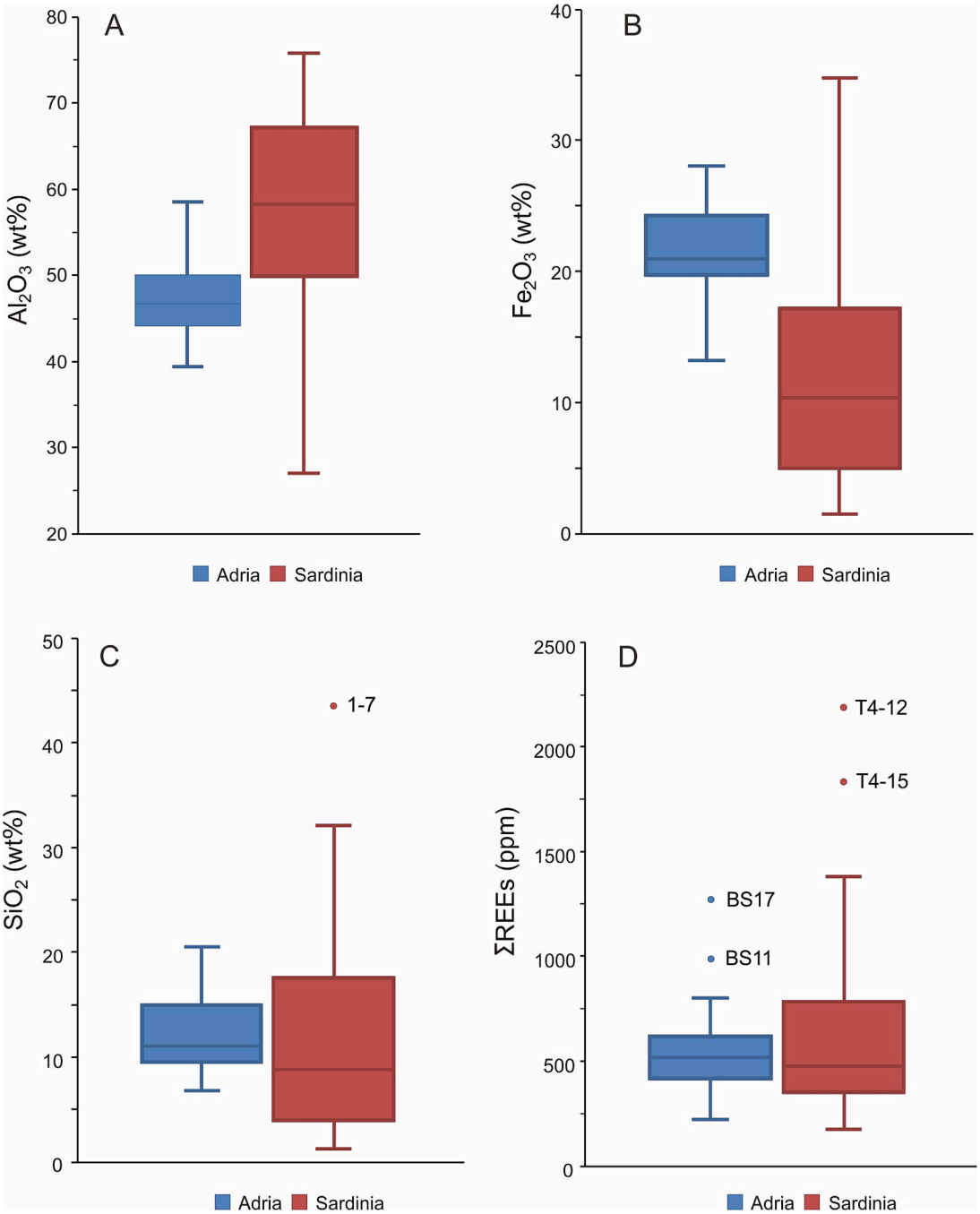

Fig. 12. Box diagram of (A) Al_2O_3 (wt%); (B) Fe_2O_3 (wt%), (C) SiO_2 (wt%) and (D) ΣREEs (ppm) of bauxite samples from Adria (n = 75) and Sardinia (n = 41). Data from (Boni et al., 2012; Mongelli et al., 2014, 2016, 2021; Mameli et al., 2007, 2020).

170 Ma) by geochronological works on ophiolites from Dinarides region, e.g., Thessaloniki ophiolite and Shebeniku massif were dated by K-Ar method at 174 ± 4.8 Ma (Boev et al., 2018) and 171 – 176 Ma (Dimo-Lahitte et al., 2001), respectively. Early – Middle Jurassic tectonic activities in the western branch of Neotethys and its companying volcanisms have been recorded in the coeval carbonate sequences of the Adria and adjacent areas involving short-lasting emersions (Vlahović et al., 2005), soft-sediment deformation (Basilone et al., 2014; Schmid et al., 2008), and tuffitic interlayers (Basilone et al., 2014). Similar to the Cretaceous zircon, Early – Middle Jurassic zircon grains also show arc-related magmatic source features, consistent with zircon trace elements and Hf isotope (-8.75 to −4.63) evidences. Early Paleozoic (430 – 470 Ma), Neoproterozoic (564 – 997 Ma) and Mesoproterozoic to Neoarchean (1542 – 2681 Ma) zircon grain ages seem to indicate a pre-Variscan origin. These zircon grains may have been brought to the Cretaceous Adria carbonate platforms by windborne detritus or erupted volcanic ashes from remelted Variscan basements of Adria (Fig. 13).

6.3. *Comparison between bauxite deposits in the Sardinia and Adria regions*

Significant differences among detrital zircon U-Pb age populations and geochemical compositions of Cretaceous bauxite deposits in the Sardinia and Adria regions indicate the diversity in parental affinities. As discussed in Section 6.2, Cretaceous bauxite deposits of Sardinia show consistency of with the Variscan basement. In Adria bauxite

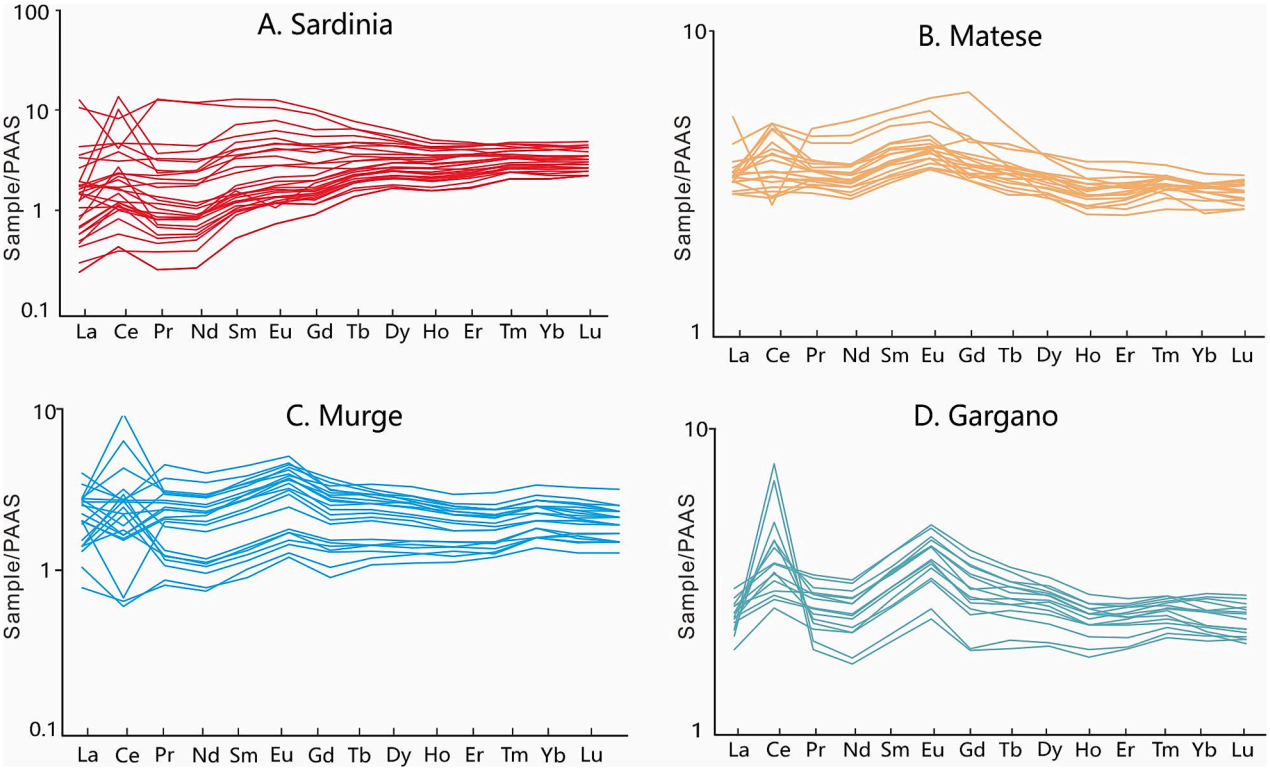

Fig. 13. PAAS-normalized REE patterns of (A) Sardinia and (B-D) Adria. Data from (Boni et al., 2012; Mongelli et al., 2014; 2016, 2021; Mameli et al., 2007, 2020).

deposits, however, zircon population reveals a more complicated scenario. This differentiation is reflected in the multi-dimensional scaling plot (Fig. 9A), in which the bauxite samples of Adria and Sardinia are roughly separated into two groups, indicating that they were derived from different source rock(s). In the Cumulative proportion plot of the "depositional lag time" (Fig. 9B), the Sardinia and Adria bauxite samples also show disparity, the four Sardinian samples acquired similar cumulative curves, while the Adrian samples contains more depositional-age grains, suggesting increasing influence from the coeval volcanic materials. In the geochemical discriminative diagrams (Sm/Nd – Eu/Eu*, Ni – Cr and U/Th – Eu/Eu*, Fig. 10), published data from bauxite samples of Adria and Sardinia regions fall into two slightly overlapped zones, indicating differences in the parental affinities. The Adria bauxite likely derives from a mixture of sources andesite and sedimentary clastic rocks (dual provenances form Adria and Dinarides). The Sardinia bauxite, instead, shows closer linkage with the Variscan metamorphic basement and its sedimentary clastic rocks cover (Fig. 14).

Although many factors can affect the geochemical composition of bauxite deposits, diversity in parent rock(s) may induce variations of geochemical compositions, and further influencing the ore quality (Bárdossy, 1982). Several studies demonstrated that the Carboniferous bauxite deposits in northern and southern North China Craton show some geochemical differences due to weathering materials from the Qinling Orogeny and Central Asia Orogeny (Wang et al., 2016), and Permian bauxite deposits in southwestern South China Craton (SCC) show geochemical variations due to multiple volcanic ashes (the Emeishan large igneous province source vs volcanic arcs source in the margin of SCC) input (Yu et al., 2016). Bauxite deposits in Sardinia and Adria also show distinct compositions. In major elements, the Sardinia bauxite contains higher Al_2O_3 (median = 58 wt%), lower Fe_2O_3 (median = 11 wt%) and SiO_2 (median = 8 wt%) than Adria bauxite (median of Al_2O_3 = 47 wt%, median of Fe_2O_3 = 22 wt%, median of SiO_2 = 12 wt %,). Further, the Sardinia bauxite has lower total contents of REE than Adria (median of ΣREE = 460 ppm for Sardinia and median of ΣREE = 505 ppm for Adria), but ΣREE in Sardinia bauxite deposits present larger variations than in the Adria ones. However, both Adria and Sardinia bauxites share some typical features of bauxite deposits in the PAAS-normalized REE patterns (e.g., enriched and flat HREEs and positive Ce anomaly), very similar to other bauxite deposits such as Permian bauxite deposits in SCC (Wang et al., 2010a, 2013). On the other hand, Sardinia bauxite samples contain larger variations (both enrichment and depletion) in LREEs, while Adria samples acquire general positive Eu anomaly and enrichment of MREEs in some samples. The specific REEs features of Adria bauxite deposits may be due to significant input of volcanic ashes, similarly to what observed for the Permian bauxite deposits in southwestern SCC (Dai et al., 2018; Zhao et al., 2013).

6.4. *Implication for Cretaceous paleogeography and tectonic evolution of Alpine Tethys*

Cretaceous bauxite deposits in the *peri*-mediterranean realm have been considered as the result of extremely favorable tectonic, paleoclimatic and paleogeographic conditions (Combes and Bárdossy, 1996; Mindszenty et al., 1995). The Alpine Tethys reached the western Mediterranean region since Middle Jurassic (Stampfli, 2000; Stampfli and Borel, 2004). During the Cretaceous, the NE-directed convergence of the Africa Plate and the Eurasian Plate resulted in the west-directed subduction of the Adria Plate beneath the future Sardinia and Corsica microplates (Carmignani et al 1995 Oggiano et al. 2009) on the western part, and the NNE-trending subduction in the West Vardar oceanic plate on the eastern part (Handy et al., 2010). Subduction-convergence led to the accretion of oceanic units over the continental margin (Sirevaag et al., 2016). The Adria Plate and the Sardinia crust were located at the paleotropic region (paleolatitude at 10°N – 30°N) during Cretaceous (Schettino and Turco, 2011), chemical weathering was further strengthened by the Cretaceous greenhouse condition (Bottini and Erba, 2018). Paleogeographically, a series of continental marginal carbonate platforms (e.g., Sardinia Platform) and isolated carbonate platforms (e.g., Apulia Platform and Apennine Carbonate Platform) were separated by inter-platform basins (Patacca and Scandone, 2007). Sequences of

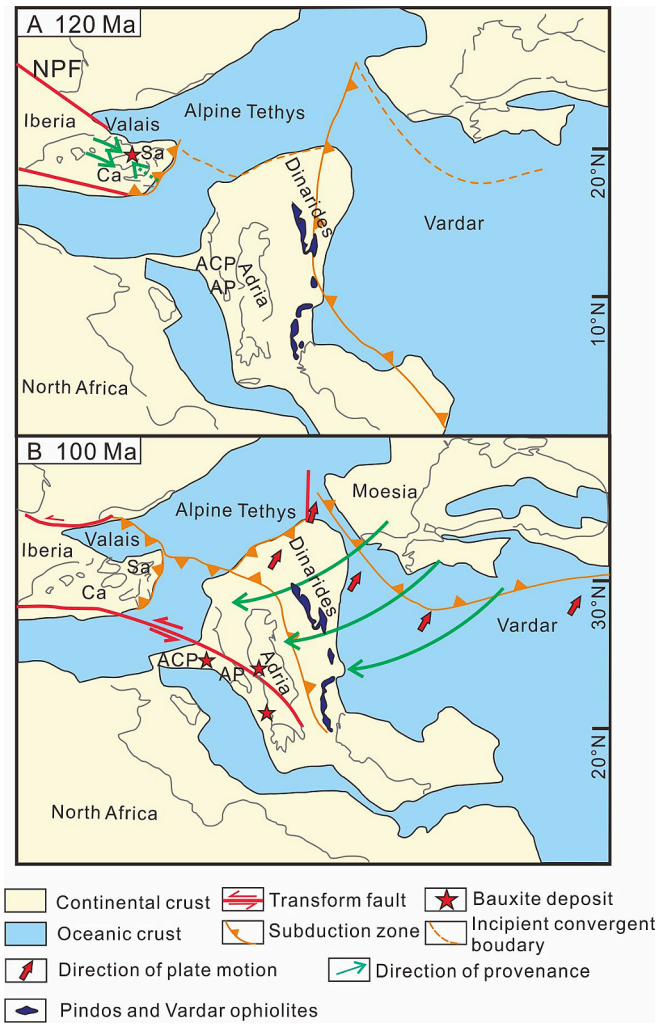

Fig. 14. Paleogeographic maps and simplified tectonic units of (A) Aptian (~120 Ma) and (B) Cenomanian (~100 Ma) in Alpine Tethys and its adjacent areas, modified after Schettino and Turco (2011). For abbreviation: ACP = Apennine Carbonate Platform; AP = Apulian Platform; Ca = Calabria; NPF = North Pyrenean fault; Sa = Sardinia.

carbonate platforms show the sensitive response for the tectonic activities, long-lasting emersions (bauxite deposits) and short-lasting emersions (thin carbonate breccia beds) were linked with regional uplifts (Vlahović et al., 2005). Based on our new detrital zircon provenance results, bauxite deposits in Adria and Sardinia regions provide further clues for tectonic and paleogeographic reconstructions of the Cretaceous Alpine Tethys.

During Early-Upper Cretaceous (Aptian – Turonian), Sardinia underwent strong uplift and emergence that caused the erosion of the Mesozoic carbonate deposit (the total thickness is at least 1.5–2 km), leading to the karstification. This uplift was probably due to the convergent boundary at the eastern margin of Iberia, where Ligurian oceanic crust began to subduct (Schettino and Turco, 2011; Mameli et al., 2020). Uplifting altitude was various in different areas of Sardinia (in pre-drift coordinates). The regions bounding Sardinia to the Northwest experienced the most severe karstification that resulted in the vanish of the whole Mesozoic carbonate deposit and the exposure of the underlying Variscan basements (Mameli et al., 2020). In western Sardinia, uplift and karstification were weaker, the carbonate platform was eroded down to the Upper Jurassic (Oxfordian) dolostone. The resulting paleosurface became the footwall of bauxite depoists, after the denudation of about 400-m-thick carbonate succession (Mameli et al., 2007).

Previous study located Sardinia on the prolongation of the Durancian isthmus during Cretaceous, and consider the Massif Meridional (as the structural relics in the allochthonous slices of basement in the Maure Massive and in basement outcrops buried in the Ligure-Provencal basin) was the main source area for bauxite deposits in Sardinia (Mameli et al., 2020). New zircon age data in this study support this statement for the high similarity in the detrital zircon populations between bauxite deposits and Variscan basements, which show the obvious difference from zircon age population that preserved in Cretaceous clastic rocks of western Pyrenees (Fig. 11F, Hart et al., 2016). Further, our data on a single Upper Cretaceous zircon indicate that Early Cretaceous volcanic ash also reached Sardinia from the West, which may come from the rifted western margin of Iberia (Garcia-Mondejar et al., 2018).

From Early Cretaceous to Late Cretaceous, the Vardar Ocean shrank due to the N- to NE-directed subduction of the Vardar oceanic crust beneath the Eurasia Plate (Robertson et al., 2013). Meanwhile, the NNE-trending subduction of the Adria Plate to the West Vardar oceanic plate resulted in formation of the ophiolites in the suture zone and the calcalkaline igneous rocks related to the back-arc environment in the Dinarides (Schmid et al., 2008). Published and new detrital zircon populations in bauxite deposits of Adria are comparable to the Cretaceous Bosnian Flysch, which was deposited in the basin between the Adriatic carbonate Platform and the Dinaride Ophiolite Zone (Mikes et al., 2008), but differed from the Gorgoglione Flysch sandstones in Southern Apennines which sourced from the Variscan basement identifiable as the Sardinia–Corsica area (Fornelli et al., 2020). The obvious difference in the basinal provenances on western and eastern sides of carbonate platforms supports the eastern provenance model for the bauxite deposits developed on the carbonate platforms. Considering the low paleolatitude of Adria Plate (20°N – 30°N) during Late Cretaceous, it was in the intertropical convergence zone and should be under the influence of southwest-directed winds (Schettino and Turco, 2011). This assumption is consistent with results of the numerical simulation of the Cretaceous Tethys based on atmospheric general circulation model (GCM), in which a circumglobal tropical current flowed westward through the continental configuration of that time (Bush, 1997).

Finally, the parental affinity existing between the Apulia (Spinazzola, Otranto Gargano) and Matese (Dragoni) samples, allows locating both the related bauxite deposits in the Mesozoic platform of Adria. This paleogeographic pertinence excludes that the carbonate platforms involved in the central-southern Apennines, before the Cenozoic collision, were located in the European (i.e., Sardinian) margin, as recently hypothesized by Arragoni et al. (2018).

7. Conclusions

(1) Prominent difference of parental affinities is observed in Cretaceous bauxite deposits of Sardinia and Adria, Italy. Dominant Early Paleozoic aged zircon grains and their various Hf isotope compositions in the Sardinia bauxite deposit reveal a supply related to the erosion and weathering of Variscan metasedimentary basement. Bauxite deposits in Adria show, instead, abundant Jurassic – Cretaceous zircon grains with negative εHf(t) values, supporting the significant supply from coeval volcanic materials.

(2) Diversity in the parent rock(s) of bauxite deposits of Adria and Sardinia led to the geochemical variation of bauxite ores. Quality of bauxite ore of Sardinia is better than Adria, generally containing higher Al and lower Fe and Si. In the PAAS-normalized REE patterns, positive Ce anomalies and flat HREEs distribution are observed in most samples. Moreover, Sardinia bauxite shows larger variation in LREEs whereas Adria bauxite present positive Eu anomaly.

(3) Cretaceous bauxite samples from Sardinia and Adria shed light on paleogeographic restoration and tectonic evolution of Alpine Tethys. During Early Cretaceous, Sardinia was affected by uplift

due to the subduction between Ligurian oceanic crust and the Iberia plate. The Mesozoic carbonate deposits were eroded and the underlying Variscan metasedimentary basement was exposed in northern Sardinia and the Massif Meridional, provided weathering materials for bauxitization in NW Sardinia. Late Cretaceous witnessed the further NNE-trending subduction of the Adria Plate to the West Vardar oceanic plate, where calcalkaline igneous rocks and volcanic ashes from Dinarides supplied weathering materials to the carbonate platforms in Adria through the wind transportation.

(4) The bauxite of central-southern Apennine does not show any Sardinian feature. As a consequence, the hosting carbonate sequence was not located on the Sardinia shelf before the Cenozoic tectonic that involved the south Mediterranean realm.

Declaration of Competing Interest

The authors declare that they have no known competing financial interests or personal relationships that could have appeared to influence the work reported in this paper.

Data availability

The data that has been used is confidential.

Acknowledgements

This study was supported by the National Key R&D Program of China (2022YFF0800200), National Natural Science Foundation of China U1812402, MOST Special Fund (MSFGPMR33) from the State Key Laboratory of GPMR, the CUG Scholar Scientific Research Funds (Project No. 2022036), and the Open Fund of the Key Laboratory of Guangdong Provincial Key Laboratory of Geodynamics and Geohazards. The Regione Autonoma della Sardegna, L.R. 7/2007, research programme "Il blocco Sardo–Corso: area chiave per la ricostruzione della geodinamica varisica" CUP J81G17000110002 - Oggiano/Mameli and University of Sassari, Fondo di Ateneo per la Ricerca 2020 - Mameli."

Appendix A. Supplementary data

Supplementary data to this article can be found online at https://doi.org/10.1016/j.oregeorev.2022.105272.

References

Abedini, A., Mongelli, G., Khosravi, M., Sinisi, R., 2020. Geochemistry and secular trends in the middle-late Permian karst bauxite deposits, northwestern Iran. Ore Geol. Rev. 124, 103660.

Abedini, A., Mongelli, G., Khosravi, M., 2021. Geochemical constraints on the middle Triassic Kani Zarrineh karst bauxite deposit, Irano-Himalayan belt, NW Iran: implications for elemental fractionation and parental affinity. Ore Geol. Rev. 133, 104099.

Abedini, A., Mongelli, G., Khosravi, M., 2022. Geochemistry of the early Jurassic Soleiman Kandi karst bauxite deposit, Irano-Himalayan belt, NW Iran: constraints on bauxite genesis and the distribution of critical raw materials. J. Geochem. Explor. 241, 107056.

Alvarez, W., 1972. Rotation of the Corsica-Sardinia microplate. Nat. Phys. Sci. 235 (58), 103–105.

Álvaro, J.J., Sánchez-García, T., Puddu, C., Casas, J.M., Díez-Montes, A., Liesa, M., Oggiano, G., 2020. Comparative geochemical study on Furongian–earliest Ordovician (Toledanian) and Ordovician (Sardic) felsic magmatic events in southwestern Europe: underplating of hot mafic magmas linked to the opening of the Rheic Ocean. Solid Earth 11, 2377–2409.

Arboit, F., Chew, D., Visoná, D., Massironi, M., Sciascia, F., Benedetti, G., Rodani, S., 2019. The geodynamic evolution of the Italian South Alpine basement from the Ediacaran to the Carboniferous: was the South Alpine terrane part of the peri-Gondwana arc-forming terranes? Gondwana Res 65, 17–30.

Arragoni, S., Fernández, L., Cuesta, A.M., Cianfarra, P., Salvini, F., 2018. Origin of exotic clasts in the Central-Southern Apennines: Clues to the Cenozoic fold-and-thrust collisional belt in the Central Mediterranean area. Geol. Mag. 155 (2), 479–505.

Avigad, D., Abbo, A., Gerdes, A., 2016. Origin of the Eastern Mediterranean: neotethys rifting along a cryptic Cadomian suture with Afro-Arabia. GSA Bull. 128, 1286–1296.

Azor, A., Martínez Poyatos, D., Accotto, C., Simancas, F., González Lodeiro, F., Talavera, C., Evans, N.J., 2021. Transcurrent displacement of the Cadomian magmatic arc. Precambr. Res. 361, 106251.

Ballèvre, M., Le Goff, E., Hébert, R., 2001. The tectonothermal evolution of the Cadomian belt of northern Brittany, France: a Neoproterozoic volcanic arc. Tectonophysics 331, 19–43.

Bárdossy, G., 1982. Karst Bauxites: Bauxite Deposits on Carbonate Rocks. Elsevier, Amsterdam.

Bárdossy, G., Combes, P.J., 1999. Karst Bauxites: Interfingering of Deposition and Palaeoweathering. In: Thiry, M., Simon-Coinçon, R. (Eds.), Palaeoweathering, Palaeosurfaces and Related Continental Deposits. Blackwell Publishing Ltd., Oxford, UK, pp. 189–206.

Basilone, L., Lena, G., Gasparo-Morticelli, M., 2014. Synsedimentary-tectonic, soft-sediment deformation and volcanism in the rifted Tethyan margin from the Upper Triassic-Middle Jurassic deep-water carbonates in Central Sicily. Sed. Geol. 308, 63–79.

Bernoulli, D., Schaltegger, U., Stern, W.B., Frey, Caron, M., Monechi, S., 2004. Volcanic ash layers in the Upper Cretaceous of the Central Apennines and a numerical age for the early Campanian. Int. J. Earth Sci. 93, 384–399.

Boev, B., Cvetković, V., Prelević, D., Šarić, K., Boev, I., 2018. East Vardar ophiolites revisited: A brief synthesis of geology and geochemical data. contributions. Section of Natural, Mathematical and Biotechnical Sciences, MASA, Vo 39, 51–68.

Bogatyrev, B., Zhukov, V., 2009. Bauxite provinces of the world. Geol. Ore Deposits 51, 339–355.

Boni, M., Reddy, S.M., Mondillo, N., Balassone, G., Taylor, R., 2012. A distant magmatic source for Cretaceous karst bauxites of Southern Apennines (Italy), revealed through SHRIMP zircon age dating. Terra Nova 24, 326–332.

Bottini, C., Erba, E., 2018. Mid-Cretaceous paleoenvironmental changes in the western Tethys. Clim. Past 14, 1147–1163.

Buccione, R., Mongelli, G., Sinisi, R., Boni, M., 2016. Relationship between geometric parameters and compositional data: a new approach to karst bauxites exploration. J. Geochem. Explor. 169, 192–201.

Bush, A.B.G., (1997). Numerical Simulation of the Cretaceous Tethys Circumglobal Current. Science 275, 807-810.

Cappelli, B. (1991) LP-HT Metamorphic core complexes in the nappe zone of the Hercynian Chain in Sardinia (Italy). In: Geologia del Basamento Italiano, Siena 21-22 marzo 1991.

Carmignani, L., Decandia, F.A., Disperati, L., Fantozzi, P.L., Lazzarotto, A., Liotta, D., et al., 1995. Relationships between the tertiary structural evolution of the Sardinia-Corsica-Provencal domain and the northern Apennines. Terra Nova 7, 128–137. https://doi.org/10.1111/j.1365-3121.1995.tb00681.x.

Casini, L., Cuccuru, S., Puccini, A., Oggiano, G., Rossi, P., 2015. Evolution of the Corsica-Sardinia Batholith and late-orogenic shearing of the Variscides. Tectonophysics 646, 65–78.

Channell, J.E.T., Muttoni, G., Kent, D.V., 2022. Adria in Mediterranean paleogeography, the origin of the Ionian Sea, and Permo-Triassic configurations of Pangea. Earth Sci. Rev. 230, 104045.

Cocherie, A., Rossi, P., Fanning, C.M., Guerrot, C., 2005. Comparative use of TIMS and SHRIMP for U-Pb zircon dating of A-type granites and mafic tholeiitic layered complexes and dykes from the Corsican Batholith (France). Lithos 82, 185–219.

Cocco, F., Funedda, A., 2017. The Sardic Phase: field evidence of Ordovician tectonics in SE Sardinia, Italy. Geol. Mag. 156, 25–38.

Combes, P.J., Bárdossy, G., 1996. Geodynamics of Bauxites in the Tethyan Realm. In: Nairn, A.E.M., Ricou, L.-.E., Vrielynck, B., Dercourt, J. (Eds.), The Tethys Ocean. Springer, US, Boston, MA, pp. 347–365.

Combes, P.J., Oggiano, G., Temussi, I., 1993. Geodynamique des bauxites sardes: typologie, génese et controle paleotectonique. Comptes Rendus de l'Académie des Sciences, Sèrie II 316, 403–409.

Corfu, F., Hanchar, J.M., Hoskin, P.W.O., Kinny, P., 2003. Atlas of zircon textures. Rev. Mineral. Geochem. 53, 469–500.

Cortesogno, L., Cassinis, G., Dallagiovanna, G., Gaggero, L., Oggiano, G., Ronchi, A., Vanossi, M., 1998. The Variscan post-collisional volcanism in late Car boniferous–Permian sequences of Ligurian Alps, southern Alps and Sardinia (Ita ly): a synthesis. Lithos 45, 305–328.

Cruciani, G., Montomoli, C., Carosi, R., Franceschelli, M., Puxeddu, M., 2015. Continental collision from two perspectives: a review of Variscan metamorphism and deformation in northern Sardinia. Periodico di mineralogia 84, 657–699.

D'Argenio, B., Mindszenty, A., 1995. Bauxites and related paleokarst: tectonic and climatic event markers at regional unconformities. Eclogae Geol. Helv. 88, 453–499.

Dai, S., Nechaev, V.P., Chekryzhov, I.Y., Zhao, L., Vysotskiy, S.V., Graham, I., Ward, C.R., Ignatiev, A.V., Velivetskaya, T.A., Zhao, L., French, D., Hower, J.C., 2018. A model for Nb–Zr–REE–Ga enrichment in Lopingian altered alkaline volcanic ashes: key evidence of H-O isotopes. Lithos 302–303, 359–369.

Deng, J., Wang, Q., Yang, S., Liu, X., Zhang, Q., Yang, L., Yang, Y., 2010. Genetic relationship between the Emeishan plume and the bauxite deposits in Western Guangxi, China: constraints from U-Pb and Lu–Hf isotopes of the detrital zircons in bauxite ores. J. Asian Earth Sci. 37, 412–424.

Dewey, J.F., Helman, M.L., Knott, S.D., Turco, E., Hutton, D.H.W., 1989. Kinematics of the western Mediterranean. Geol. Soc. London, Spec. Publ. 45, 265–283.

Dimo-Lahitte, A., Monié, P., Vergély, P., 2001. Metamorphic soles from the Albanian ophiolites: petrology, 40Ar/39Ar geochronology, and geodynamic evolution. Tectonics 20, 78–96.

Fornelli, A., Gallicchio, S., Micheletti, F., Langone, A., 2020. U-Pb detrital zircon ages from Gorgoglione Flysch sandstones in Southern Apennines (Italy) as provenance indicators. Geol. Mag. 158, 859–874.
Gaggero, L., Oggiano, G., Buzzi, L., Slejko, F.F., Cortesogno, L., 2007. Post-Variscan Mafic Dikes from the late Orogenic Collapse to the Tethyan Rift: evidence from Sardinia. Ofioliti 32, 15–37.
Garcia, M.M., Carraceso-Sancez, M., Owen, H., Fernadez-Mendiola, P.A., 2018. The early aptian volcanic episode of gutiolo (N Spain: expression of the Bilbao Rift Fault Zone. Geol. J. 3509–3526.
Gretter, N., Ronchi, A., Langone, A., Perotti, C., 2013. The transition between the two major Permian tectono-stratigraphic cycles in the central Southern Alps: results from facies analysis and U/Pb geochronology. Int. J. Earth Sci. 102.
Griffin, W.L., Powell. W.J., Pearson. N.J., O'Reilly. S.Y., (2008). Glitter: Datareduction software for laser ablation ICP-MS. MineralogicalAssociation of Canada Short Course 40, Vancouver, B.C., p. 308–311.
Grimes, C.B., Wooden, J.L., Cheadle, M.J., John, B.E., 2015. "Fingerprinting" tectono-magmatic provenance using trace elements in igneous zircon. CoMP 170, 46.
Gu, J., Huang, Z., Fan, H., Ye, L., Jin, Z., 2013. Provenance of lateritic bauxite deposits in the Wuchuan–Zheng'an–Daozhen area, Northern Guizhou Province, China: LA-ICP-MS and SIMS U-Pb dating of detrital zircons. J. Asian Earth Sci. 70–71, 265–282.
Handy, M.R., Schmid, M., Bousquet, S., Kissling, R., Bernoulli, E., 2010. Reconciling plate-tectonic reconstructions of Alpine Tethys with the geological–geophysical record of spreading and subduction in the Alps. Earth-Sci. Rev. 102, 121–158.
Hart, N.R., Stockli, D.F., Hayman, N.W., 2016. Provenance evolution during progressive rifting and hyperextension using bedrock and detrital zircon U-Pb geochronology, Mauléon Basin, western Pyrenees. Geosphere 12, 1166–1186.
Hartman, J.A., 1955. Origin of heavy minerals in Jamaican bauxite. Econ. Geol. 50, 738–747.
Hawkesworth, C.J., Kemp, A.I.S., 2006. Using hafnium and oxygen isotopes in zircons to unravel the record of crustal evolution. Chem. Geol. 226, 144–162.
Hou, Y.-L., Zhong, Y.-T., Xu, Y.-G., He, B., 2017. The provenance of late Permian karstic bauxite deposits in SW China, constrained by the geochemistry of interbedded clastic rocks, and U-Pb–Hf–O isotopes of detrital zircons. Litho 278–281, 240–254.
Khosravi, M., Abedini, A., Alipour, S., Mongelli, G., 2017. The Darzi-Vali bauxite deposit, West-Azarbaidjan Province, Iran: critical metals distribution and parental affinities. J. Afr. Earth Sci. 129, 960972.
Koglin, N., Zeh, A., Franz, G., Schüssler, U., Glodny, J., Gerdes, A., Brätz, H., 2018. From Cadomian magmatic arc to Rheic ocean closure: the geochronological-geochemical record of nappe protoliths of the Münchberg Massif, NE Bavaria (Germany). Gondwana Res. 55, 135–152.
Liu, J., Zhao, Y., Liu, A., Zhang, S., Yang, Z., Zhuo, S., 2014. Origin of Late Palaeozoic bauxites in the North China Craton: constraints from zircon U-Pb geochronology and *in situ* Hf isotopes. J. Geol. Soc. 171, 695–707.
Liu, X., Wang, Q., Peng, Y., Yin, R., Ma, Y., Zhao, L., Zhang, S., 2022. Intensified and apace bauxitization over the paleo-karstic surface linked to volcanism. GSA Bull.
Ludwig, K.R., 2001. In: Center, B.G. (Ed.), ISOPLOT 3.70: A Geochronological Toolkit for Microsoft Excel. Berkeley, California.
MacLean, W., Bonavia, F., Sanna, G., 1997. Argillite debris converted to bauxite during karst weathering: evidence from immobile element geochemistry at the Olmedo Deposit, Sardinia. Mineral. Depos. 32, 607–616.
Mameli, P., Mongelli, G., Sinisi, R., Oggiano, G. (2020). Weathering Products of a Dismantled Variscan Basement. Minero-Chemical Proxies to Insight on Cretaceous Palaeogeography and Late Neogene Palaeoclimate of Sardinia (Italy). Frontiers in Earth Science 8:290 10.3389/feart.2020.00290.
Mameli, P., Mongelli, G., Oggiano, G., Dinelli, E., 2007. Geological, geochemical and mineralogical features of some bauxite deposits from Nurra (Western Sardinia, Italy): insights on conditions of formation and parental affinity. Int. J. Earth Sci. 96, 887–902.
Mikes, T., Christ, D., Petri, R., Dunkl, I., Frei, D., Báldi-Beke, M., Reitner, J., Wemmer, K., Hrvatović, H., von Eynatten, H., 2008. Provenance of the Bosnian Flysch. Swiss J. Geosci. 101, 31–54.
Mindszenty, A., D'Argenio, B., Aiello, G., 1995. Lithospheric bulges recorded by regional unconformities. The case of mesozoic-tertiary apulia. Tectonophysics 252, 137–161.
Mongelli, G., Boni, M., Buccione, R., Sinisi, R., 2014. Geochemistry of the Apulian karst bauxites (southern Italy): chemical fractionation and parental affinities. Ore Geol. Rev. 63, 9–21.
Mongelli, G., Buccione, R., Sinisi, R., 2015. Genesis of autochthonous and allochthonous Apulian karst bauxites (Southern Italy): climate constraints. Sediment. Geol. 325, 168–176.
Mongelli, G., Buccione, R., Gueguen, E., Langone, A., Sinisi, R., 2016. Geochemistry of the Apulian allochthonous karst bauxite, Southern Italy: distribution of critical elements and constraints on Late Cretaceous Peri-Tethyan palaeogeography. Ore Geol. Rev. 77, 246–259.
Mongelli, G., Boni, M., Oggiano, G., Mameli, P., Sinisi, R., Buccione, R., Mondillo, N., 2017. Critical metals distribution in Tethyan karst bauxite: the cretaceous Italian ores. Ore Geol. Rev. 86, 526–536.
Mongelli, G., Mameli, P., Sinisi, R., Buccione, R., Oggiano, G., 2021. REEs and other critical raw materials in Cretaceous Mediterranean-type bauxite: the case of the Sardinian ore (Italy). Ore Geol. Rev. 139, 104559.
Montes, A.D., Catalán, J.R.M., Mulas, F.B., 2010. Role of the Ollo de Sapo massive felsic volcanism of NW Iberia in the Early Ordovician dynamics of northern Gondwana. Gondwana Res. 17, 363–376.
Oggiano, G., Funedda, A., Carmignani, L., Pasci, S., 2009. The Sardinia-Corsica microplate and its role in the Northern Apennine Geodynamics: new insights from the Tertiary intraplate strike-slip tectonics of Sardinia. Boll. Soc. Geol. Ital. 128 (2), 527–539. https://doi.org/10.3301/IJG.2009.128.2.527.
Oggiano, G., Gaggero, L., Funedda, A., Buzzi, L., Tiepolo, M., 2010. Multiple early Paleozoic volcanic events at the northern Gondwana margin: U-Pb age evidence from the Southern Variscan branch (Sardinia, Italy). Gondwana Res. 17, 44–58.
Paoli, G., Stokke, H.H., Rocchi, S., Sirevaag, H., Ksienzyk, A.K., Jacobs, J., Košler, J., 2017. Basement provenance revealed by U-Pb detrital zircon ages: a tale of African and European heritage in Tuscany, Italy. Lithos 277, 376–387.
Patacca, E., Scandone, P., 2007. Geology of the Southern Apennines. Bollettino- Societa Geol. Italiana 7, 75–112.
Price, G.D., Valdes, P.J., Sellwood, B.W., 1997. Prediction of modern bauxite occurrence: implications for climate reconstruction. Palaeogeogr. Palaeoclimatol. Palaeoecol. 131, 1–13.
Robertson, A.H.F., Trivić, B., Đerić, N., Bucur, I.I., 2013. Tectonic development of the Vardar ocean and its margins: evidence from the Republic of Macedonia and Greek Macedonia. Tectonophysics 595–596, 25–54.
Rossi, P., Cocherie, A., 1991. Genesis of a Variscan batholith: field, petrological and mineralogical evidence from the Corsica-Sardinia batholith. Tectonophysics 195, 319–346.
Rossi, P., Oggiano, G., Cocherie, A., 2009. A restored section of the "southern Variscan realm" across the Corsica-Sardinia microcontinent. C. R. Geosci. 341, 224–238.
Rubatto, D., 2002. Zircon trace element geochemistry: partitioning with garnet and the link between U-Pb ages and metamorphism. Chem. Geol. 184, 123–138.
Scherreiks, R., BouDagher-Fadel, M. (2021). The closure of the Vardar ocean (the western domain of the northern Neotethys) from early Middle Jurassic to Paleocene time, based on surface geology of eastern Pelagonia and the Vardar zone, biostratigraphy, and seismic-tomographic images of the mantle below the Central Hellenides. UCL Open Eviron. 3, 10.14324/14111.14444/ucloe.000024.
Scherreiks, R., Bosence, D., BouDagher-Fadel, M., Meléndez, G., Baumgartner, P.O., 2010. Evolution of the Pelagonian carbonate platform complex and the adjacent oceanic realm in response to plate tectonic forcing (Late Triassic and Jurassic), Evvoia, Greece. Int. J. Earth Sci. 99, 1317–1334.
Schettino, A., Turco, E., 2011. Tectonic history of the western Tethys since the Late Triassic. GSA Bull. 123, 89–105.
Schmid, S.M., Bernoulli, D., Fügenschuh, B., Matenco, L., Schefer, S., Schuster, R., Tischler, M., Ustaszewski, K., 2008. The Alpine-Carpathian-Dinaridic orogenic system: correlation and evolution of tectonic units. Swiss J. Geosci. 101, 139–183.
Schreiber, D., Giannerini, G., Lardeaux, J.M., 2011. The Southeast France basin during late cretaceous times: the spatiotemporal link between pyrenean collision and alpine subduction. Geodin. Acta 24, 21–35. https://doi.org/10.3166/ga.24.21-35.
Scrocca, D., Carminati, E., Doglioni, C., (2005). Deep structure of the southern Apennines, Italy: Thin-skinned or thick-skinned? Tectonics 24.
Secchi, F., Giovanardi, T., Naitza, S., Casalini, M., Kohút, M., Conte, A.M., Oggiano, G., 2022. Multiple crustal and mantle inputs in post-collisional magmatism: evidence from late-Variscan Sàrrabus pluton (SE Sardinia, Italy). Lithos 420, 106697.
Sinisi, R., 2018. Mineralogical and geochemical features of Cretaceous Bauxite from San Giovanni Rotondo (Apulia, Southern Italy): a provenance tool. Minerals 8, 567.
Sirevaag, H., Jacobs, J., Ksienzyk, A.K., Rocchi, S., Paoli, G., Jørgensen, H., Košler, J., 2016. From Gondwana to Europe: the journey of Elba Island (Italy) as recorded by U-Pb detrital zircon ages of Paleozoic metasedimentary rocks. Gondwana Res. 38, 273–288.
Speranza, F., Villa, I.M., Sagnotti, L., Florindo, F., Cosentino, D., Cipollari, P., Mattei, M., 2002. Age of the Corsica-Sardinia rotation and Liguro-Provençal Basin spreading: new paleomagnetic and Ar/Ar evidence. Tectonophysics 347 (4), 231–251.
Stampfli, G.M., Borel, G.D., (2004). The TRANSMED Transects in Space and Time: Constraints on the Paleotectonic Evolution of the Mediterranean Domain, in: Cavazza, W., Roure, F., Spakman, W., Stampfli, G.M., Ziegler, P.A. (Eds.). The TRANSMED Atlas. The Mediterranean Region from Crust to Mantle: Geological and Geophysical Framework of the Mediterranean and the Surrounding Areas. Springer Berlin Heidelberg, Berlin, Heidelberg, pp. 53-80.
Stampfli, G.M., (2000). Tethyan oceans, in: Bozkurt, E., Winchester, J.A., Piper, J.D.A. (Eds.), Tectonics and Magmatism in Turkey and the Surrounding Area. Geological Society of London, p. 0.
Sudom, M.D., St. Arnaud, R.J., 1971. Use of quartz, zirconium and titanium as indices in pedological studies. CaJSS 51, 385–396.
Vermeesch, P., 2004. How many grains are needed for a provenance study? Earth Planet. Sci. Lett. 224, 441–451.
Vitale, S., Amore, O.F., Ciarcia, S., Fedele, L., Grifa, C., Prinzi, E.P., Tavani, S., Tramparulo, F.D.A., 2018. Structural, stratigraphic, and petrological clues for a Cretaceous-Paleogene abortive rift in the southern Adria domain (southern Apennines, Italy). Geol J. 53, 660–681.
Vlahović, I., Tišljar, J., Velić, I., Matičec, D., 2005. Evolution of the Adriatic Carbonate Platform: palaeogeography, main events and depositional dynamics. Palaeogeogr. Palaeoclimatol. Palaeoecol. 220, 333–360.
von Raumer, J.F., Bussy, F., Schaltegger, U., Schulz, B., Stampfli, G.M., 2013. Pre-Mesozoic Alpine basements—their place in the European Paleozoic framework. GSA Bull. 125, 89–108.
von Raumer, J.F., Stampfli, G.M., Arenas, R., Sánchez Martínez, S., 2015. Ediacaran to Cambrian oceanic rocks of the Gondwana margin and their tectonic interpretation. Int. J. Earth Sci. 104, 1107–1121.
Wang, Q., Deng, J., Liu, X., Zhang, Q., Sun, S., Jiang, C., Zhou, F., 2010a. Discovery of the REE minerals and its geological significance in the Quyang bauxite deposit, West Guangxi, China. J. Asian Earth Sci. 39, 701–712.
Wang, Q., Deng, J., Liu, X., Zhao, R., Cai, S., 2016. Provenance of Late Carboniferous bauxite deposits in the North China Craton: new constraints on marginal arc construction and accretion processes. Gondwana Res. 38, 86–98.
Wang, X., Jiao, Y., Du, Y., Ling, W., Wu, L., Cui, T., Zhou, Q., Jin, Z., Lei, Z., Weng, S., 2013. Rare earth element (REE) mobility and Ce anomaly in bauxite deposit of

Wuchuan-Zheng'an-Daozhen Area, Northern Guizhou, China. J. Geochem. Explor. 133, 103–117.
Wang, Y., Zhou, L., Zhao, L., Ji, M., Gao, H., 2010b. Palaeozoic uplands and unconformity in the North China Block: constraints from zircon LA-ICP-MS dating and geochemical analysis of Bauxite. Terra Nova 22, 264–273.
Weng, S., Yu, W., Algeo, T.J., Du, Y., Li, P., Lei, Z., Zhao, S., 2019. Giant bauxite deposits of South China: multistage formation linked to Late Paleozoic Ice Age (LPIA) eustatic fluctuations. Ore Geol. Rev. 104, 1–13.
Wang, Q., Yang, L., Xu, X., Santosh, M., Wang, Y., Wang, T., Chen, F., Wang, R., Gao, L., Liu, X., Yang, S., Zeng, Y., Chen, J., Zhang, Q., Deng, J., 2020. Multi-stage tectonics and metallogeny associated with Phanerozoic evolution of the South China Block: A holistic perspective from the Youjiang Basin. Earth Sci. Rev. 211, 103405.
Xiong, G., Yu, W., Du, Y., Weng, S., Pang, D., Deng, X., Zhou, J., 2021. Provenance of Lower Carboniferous Bauxite Deposits in Northern Guizhou, China: constraints from geochemistry and detrital zircon U-Pb ages. J. Earth Sci. 32, 235–252.
Yang, J., Cawood, P.A., Du, Y., Huang, H., Huang, H., Tao, P., 2012. Large Igneous Province and magmatic arc sourced Permian-Triassic volcanogenic sediments in China. Sediment. Geol. 261–262, 120–131.
Yang, S., Wang, Q., Zhang, Q., Chen, J., Huang, Y., 2018. Terrestrial deposition processes of Quaternary gibbsite nodules in the Yongjiang Basin, southeastern margin of Tibet, and implication for the genesis of ancient karst bauxite. Sediment. Geol. 373, 292–306.
Young, G.M., Nesbitt, H.W., 1998. Processes controlling the distribution of Ti and Al in weathering profiles, siliciclastic sediments and sedimentary rocks. J. Sediment. Res. 68, 448–455.
Yu, W., Algeo, T.J., Du, Y., Zhang, Q., Liang, Y., 2016. Mixed volcanogenic–lithogenic sources for Permian bauxite deposits in southwestern Youjiang Basin, South China, and their metallogenic significance. Sediment. Geol. 341, 276–288.
Yu, W., Algeo, T.J., Yan, J., Yang, J., Du, Y., Huang, X., Weng, S., 2019. Climatic and hydrologic controls on upper Paleozoic bauxite deposits in South China. Earth-Sci. Rev. 189, 159–176.
Žák, J., Sláma, J., 2018. How far did the Cadomian terranes travel from Gondwana during early Palaeozoic? A critical reappraisal based on detrital zircon geochronology. Int. Geol. Rev. 60, 319–338.
Zhao, L., Chen, Z.-Q., Algeo, T.J., Chen, J., Chen, Y., Tong, J., Gao, S., Zhou, L., Hu, Z., Liu, Y., 2013. Rare-earth element patterns in conodont albid crowns: evidence for massive inputs of volcanic ash during the latest Permian biocrisis? Glob. Planet. Change 105, 135–151.
Zhou, J., Yu, W., Du, Y., Liu, X., Wang, Y., Xiong, G., Zhao, Z., Pang, D., Shen, D., Weng, S., Liu, Z., Chen, D., 2022. Provenance change and continental weathering of Late Permian bauxitic claystone in Guizhou Province, Southwest China. J. Geochem. Explor. 236, 106962.